UNIVERSIDADE FEDERAL DE PERNAMBUCO
DEPARTAMENTO DE FÍSICA - CCEN
PROGRAMA DE PÓS-GRADUAÇÃO EM FÍSICA

LEA LUISE MADUREIRA LAUTENBACHER

INVERTING NON-BIJECTIVE MAPS THROUGH RECOVERING CHANNELS

Recife
2021

LEA LUISE MADUREIRA LAUTENBACHER

INVERTING NON-BIJECTIVE MAPS THROUGH RECOVERING CHANNELS

Dissertation presented with the postgraduate program in Physics at the **Universidade Federal de Pernambuco** as a partial requirement to obtain the title of **Master in Physics**.

Program of studies: Theoretical and Computational Physics.

Supervisor:

Prof. Dr. Nadja Kolb Bernardes.

Co-supervisor:

Prof. Dr. Fernando Roberto de Luna Parisio Filho.

Recife
2021

Catalogação na fonte
Bibliotecária Mariana de Souza Alves CRB4-2105

L389i Lautenbacher, Lea Luise Madureira
Inverting non-bijective maps through recovering channels/ Lea Luise Madureira Lautenbacher – 2021.
78 f.: il., fig.

Orientadora: Nadja Kolb Bernardes.
Dissertação (Mestrado) – Universidade Federal de Pernambuco. CCEN, Física, Recife, 2021.
Inclui referências e apêndices.

1. Física Teórica e Computacional. 2. Canais quânticos. 3. Mapa de recuperação Petz. 4. Grau de não-invertibilidade. I. Bernardes, Nadja Kolb (orientadora) II. Título.

530.1 CDD (22. ed.) UFPE-CCEN 2021-78

LEA LUISE MADUREIRA LAUTENBACHER

INVERTING NON-BIJECTIVE MAPS THROUGH RECOVERING CHANNELS

Dissertação apresentada junto ao programa de Pós Graduação em Física da **Universidade Federal de Pernambuco** como requisito parcial para obtenção do título de **Mestre em Física**.

Data de aprovação: 29/03/2021

Banca examinadora:

Profª. Dra. Nadja Kolb Bernardes
Orientadora, DF-UFPE

Prof. Dr. Fernando Roberto de Luna Parisio Filho
Co-orientadora, DF-UFPE

Prof. Dr. Daniel Felinto Pires Barbosa
Examinador Interno, DF-UFPE

Prof. Dr. Gabriel Teixeira Landi
Examinador Exerno, IF-USP

Aos meus pais, Nadja e Clemens.

AGRADECIMENTOS

Honestamente não sei nem por onde começar... Acredito que o mestrado foi mais uma incrível experiência do que simplesmente o trabalho aqui apresentado.

Agradeço à minha orientadora Nadja, que afinal passou a ser mais uma amiga. Obrigada por todos os conselhos, críticas, apoio e por ter me proporcionado momentos de grande aprendizado na vida acadêmica.

Agradeço a Fernando de Melo, meu colaborador com quem tive ótimas conversas e que me guiou durante todo esse trabalho.

Um agradecimento especial aos meus pais, Nadja e Clemens, a quem eu dedico esse trabalho e tudo o que eu venha a produzir na minha jornada. Graças a todo esse mais sincero amor, estou aqui hoje finalizando mais uma etapa da minha vida.

A Guilherme, obrigada por ter sido mais do que um companheiro, um grande amigo. Por me fazer rir até nos piores dias, por cuidar de mim, e me incentivar a ser a mulher que eu quero ser e a fazer o que me faz feliz.

Agradeço a Lucas, meu irmão de outros pais, que tornou leve o fato de ser a única menina da turma, desde o primeiro período da graduação. Um grande amigo, seja pra me ajudar a fazer uma conta, a escolher uma roupa, a terminar uma cerveja ou um café. Ele é o cara certo pra isso.

A Polly, a Bruna e a Aninha, obrigada pela ótima amizade, pelas risadas, pela imensa cumplicidade e por me fizeram lembrar de que nem tudo é só física e que sair pra dançar é muito necessário às vezes.

A João e Bia pelos nossos encontros, que por mais esporádicos que sejam, nunca deixam de ser memoráveis e dançantes. A Yuri, a Toni e a Bento, que fazem eu me sentir como uma pedrinha preciosa na vida deles, mal sabem que eles que são na minha. Aos meus mentores computacionais, Írio e Pedro, obrigada pelos conselhos e por uma bela amizade regada à café e risadas.

Agradeço aos professores que tanto contribuíram para a minha formação, em especial Fernando Parisio, Leonardo Cabral e Bruno Carneiro da Cunha. Obrigada por partilharem de seu conhecimento de maneira tão inspiradora, despertando meu interesse em assuntos que nunca antes tinha pensado em conhecer.

À minha família pelo suporte, em especial ao meu Tio Neilson, que me acolheu

há 6 anos atrás quando eu era apenas uma menina querendo cursar Física. Obrigada pelo apoio.

Por fim, agradeço ao Conselho Nacional de Desenvolvimento Científico e Tecnológico (CNPq), pelo suporte financeiro, sem o qual não teria sido possível a realização deste e demais importantíssimos trabalhos que contribuem para a ciência brasileira. Agradeço também ao Programa de Pós-graduação do Departamento de Física da UFPE, que me possibilitou participar de eventos científicos imprescindíveis à minha formação.

"In every job that must be done, there is an element of fun"

Mary Poppins (STEVENSON, 1964)

ABSTRACT

In this dissertation we are interested in the dynamics of open quantum systems in the context of quantum information. First, we investigate the dynamics of one qubit at the regime where an inverse evolution is not well defined. This limit is widely used and explored in this work, called as the limit of non-bijectivity. We demonstrate how to compute a completely positive inverse evolution, based on the theory of recovery maps, here to be the Petz recovery map. The analyzed evolutions are the typical decoherence processes: dephasing, depolarizing and amplitude damping channels in the regime of non-bijectivity. To measure how efficient the Petz can be recovering a random quantum state, we use the fidelity function as the figure of merit. Also, we quantify how non-invertible a dynamics is compared to another. As an application for this formalism, in the second part of this work we show how we can explore recovery maps in the context of non-Markovian evolutions, in order to minimize memory effects. We demonstrate that recovering maps can be useful under certain constraints to simulate a non-Markovian evolution by an "almost" Markovian one. We demonstrate that there exists a strong dependence between the success of this strategy and the initial correlations between system and environment.

Keywords: Quantum Channels. Petz recovery map. Non-invertibility degree. Markovian evolutions. Non-Markovian effects.

RESUMO

Nesta dissertação estamos interessados na dinâmica de sistemas quânticos abertos no contexto de informação quântica. A princípio, investigamos a dinâmica de um qubit no regime em que uma evolução inversa não está bem definida. Este limite é amplamente explorado neste trabalho, chamado de limite de não-bijetividade. Demonstramos como construir uma evolução inversa que seja um processo físico bem definido, baseado na teoria de mapas de recuperação, aqui o mapa de recuperação Petz. As evoluções analisadas são típicos processos de decoerência: dephasing, depolarizing e amplitude damping, no regime de não-bijetividade. A fim de medir o quão eficiente o Petz recupera um estado quântico aleatório, nós usamos como figura de mérito a função fidelidade. Também, quantificamos o quão não-inversível uma dinâmica é comparada a outra. Como uma aplicação doesse formalismo, na segunda parte do trabalho, mostramos como os mapas de recuperação podem ser explorados em se tratando de evoluções não-Markovianas, a fim de minimizar efeitos de memória. Demonstramos que sob certas circunstâncias os mapas de recuperação podem ser úteis para simular uma evolução não-Markoviana por uma "quase" Markoviana. Evidenciamos que existe uma forte dependência entre o sucesso da estratégia aqui proposta e as correlações iniciais entre sistema e ambiente.

Palavras-chave: Canais quânticos. Mapa de recuperação Petz. Grau de não-invertibilidade. Evoluções Markovianas. Efeitos não-Markovianos.

LIST OF FIGURES

LIST OF ABBREVIATIONS AND ACRONYMS

BLP	Breuer, Laine and Piilo
CP	Completely positive
CPTP	Completely positive and trace preserving
dim	Dimension
FWHM	Full width at half maximum
GKSL	Gorini-Kossakowski-Susarshan-Lindblad
Im	Image set
LOCC	Local operations and classical communication
NM	Non-Markovian
RHP	Rivas, Huelga and Plenio
TP	Trace preserving

TABLE OF CONTENTS

1 INTRODUCTION

"What prevents us believing that through the expansion of physical knowledge new formulas and rules will be developed, which, together with the current formal approach, will make precise predictions possible again? "

Grete Hermann

Quantum mechanics provides us tools and approaches to describe the nature at a small scale like atoms and molecules. Since the beginning of its development is surrounded by critics regarding the lack of a physical principle that justifies its peculiar behavior. In the quantum world, the outcomes of measurements, in order to characterize the system, could never be predicted with certainty (BORN, 1926). This "incompleteness" was demonstrated in 1927 with Werner-Heisenberg's uncertainty principle, by which two properties of a same system could not be determined simultaneously with precision (HEISENBERG, 1927).

Since the 1970s many techniques for controlling single quantum systems have been developed. For example, manipulations in even smaller scales, trapping a single atom in an 'atom trap', isolating it from the rest of the world and allowing us to probe many different aspects of its behavior with incredible precision (PRITCHARD, 1983). Developments both in the fundamentals of the theory and in its applications have led to the creation of the quantum information field (NIELSEN; CHUANG, 2000).

In the 1980s and 1990s, the concept of *information* has been reformulated. According to Rolf Landauer : *"Information is physical"* (LANDAUER, 1991). More precisely, information is a physical entity, subjected to the laws of nature that govern the systems where it is stored and processed. Scientists began to wonder about how information could be better processed and encoded in quantum particles and how it could be affected by the non-classical phenomena. Quantum effects became powerful resources to improve information-processing technologies.

In the last few years, with the advance of quantum computing and quantum communication, open quantum systems became an active area of research, see (NIELSEN; CHUANG, 2000; SCHUMACHER; WESTMORELAND, 2010; BREUER et al., 2002) for a deep influx to this formalism. It is very uncommon to deal with systems in complete

isolation. As a consequence of this interaction with the environment, unexpected memory effects and information losses are challenges for the development of quantum technologies.

In this work we investigate the non-bijectivity property in open quantum systems. Recently, the study of non-bijective evolutions received considerable attention (CHRUŚCIŃSKI et al., 2018; JEKNIC-DUGIC et al., 2021). A simple way to find non-bijectivity is in image non-increasing maps. Here, we study the limit of non-bijectivity, when an inverse map is not well defined, of typical one-qubit quantum channels, such as dephasing, depolarizing and amplitude damping. By their usefullness in foundational issues, it is possible to investigate crucial tools and analyze the behavior of a quantum system subjected to certain conditions that allow us to explore the concept of non-invertibility of quantum evolutions. Invertibility is a concept difficult to be addressed in open quantum systems. Based on the approach of recovering maps, we build an inverse physical map capable to recover an information that was previously lost about the system. We also provide an extensive analysis of the Petz recovery maps and its properties.

With the obtained results, we developed a tool to investigate the non-invertibility issue in non-Markovian evolutions. The notion of non-Markovian evolutions has attracted considerable attention due to the relevance in the development of new quantum technologies. In practice, physical evolutions are in fact non-Markovian, dynamics with some memory effects due to the system environment interaction. Many techniques have been used to go beyond Markovian approximations in order to better understand these memory effects. An example is the coarse graining map, when the time is discretized in bigger intervals than the correlation time of the environment. A procedure good enough to describe a variety of processes like the spontaneous emission of a two-level atom or the damping of an harmonic oscillator. It is possible to use this strategy in an attempt to recover a Markovian dynamics by coarse graining its time evolution (BERNARDES et al., 2017). In this work, we propose an approach based on the concept of CP-divisibility (RIVAS et al., 2014). We use the Petz recovery map to transform a non completely positive dynamics into a completely positive one. This technique allow us to explore the main differences between the original NM dynamics and the proposed one, including the reasons behind the memory effects. We show that using our approach is even possible to attenuate the non-Markovian behavior, and suppress strange memory effects.

1.1 THESIS OUTLINE

The focus of this work is to analyze non-bijective maps, characterizing quantum channels and exploiting non-Markovian dynamics. The thesis can be break up as follows:

1. Chapters 2 and 3 present a brief introduction to the formalism of quantum information

theory and open quantum systems, respectively.

2. Chapter 4 introduces non-bijective evolutions from a mathematical perspective and then classify the previously mentioned physical evolutions in the limit of non-bijectivity. Later is also presented the Petz recovery map approach and some useful mathematical properties.

3. In Chapter 5 we apply the Petz recovery map to develop an approach that enables us to define a physical reverse map. We compare different non-bijective maps and propose a non-invertibility degree to the analyzed quantum channels.

4. In Chapter 6 we review Markovian quantum processes. We also present proposed measures to quantify and detect non-Markovianity.

5. In Chapter 7 we apply our formalism to describe a completely positive (CP) dynamics from a non-completely positive (NCP) one. We demonstrate that depending on the evolution, the Petz recovery map approach can be useful in the study and characterization of non-Markovian dynamics.

6. The Chapter 8 consists in the discussion of new perspectives and presenting the concluding remarks.

2 QUANTUM INFORMATION: FUNDAMENTALS

"I have completely forgotten the symbolic calculus."

Emmy Noether

The main goal of this chapter is reviewing basic and essential concepts for characterizing many of the fundamental notions of quantum information theory. What is information?

There are many different answers to this question. We can summarize them as the following: *information is both the uncertainty we have about a physical system before observing it and also the knowledge we have about the system after observing it.* It is interesting that some amount of information can be carried by very different forms, or signals. Classically, the smallest unity of information is the bit. The bit is a way to describe a physical system with two possible distinguishable states 0 and 1. In the quantum world is a little bit different, but a property shared between both theories is the transformability of information. Information can be transformed. This is the central point and matter of study of information processing tasks. We begin by briefly introducing the quantum bit, the fundamental unit of information, following by mathematical and geometrical tools used to describe information processing models.

2.1 QUANTUM BITS

The state of a physical system is described by a *density operator* ρ defined on a linear space of complex vectors, known as the Hilbert space $\mathcal{H}$. The density operator, called usually as density matrix is a hermitian, trace one, positive operator acting on $\mathcal{H}$. In this work we are concerned with the study of qubits or quantum bits, a simple two-level system, which state space is $\mathcal{H} = \mathbb{C}^2$, and consequently ρ is a 2×2 matrix.

A classical bit is a unity of information that can have two values 1 or 0. Thanks to the superposition principle in quantum mechanics, the qubit can assume a superposition of values between $|0\rangle$ and $|1\rangle$. It can be described as:

$$|\psi\rangle = \alpha|0\rangle + \beta|1\rangle, \tag{1}$$

where α, β are complex numbers and $|\alpha|^2 + |\beta|^2 = 1$, since they are probabilistic coefficients, and $\langle\psi|\psi\rangle = 1$. A measurement can be performed on this qubit leaving it in the

corresponding state $|0\rangle$ or $|1\rangle$ with respective probabilities $|\alpha|^2$ and $|\beta|^2$. The states $|0\rangle$ and $|1\rangle$ are known as a computational basis states.

The basis is a reference set of orthonormal states. For this work, it is worth to mention the following standard operators, called Pauli operators, written in this basis

$$\sigma_0 \equiv \begin{pmatrix} 1 & 0 \\ 0 & 1 \end{pmatrix}; \qquad \sigma_1 \equiv \begin{pmatrix} 0 & 1 \\ 1 & 0 \end{pmatrix}; \tag{2}$$

$$\sigma_2 \equiv \begin{pmatrix} 0 & -i \\ i & 0 \end{pmatrix} \qquad \sigma_3 \equiv \begin{pmatrix} 1 & 0 \\ 0 & -1 \end{pmatrix}. \tag{3}$$

The Pauli operators are examples of quantum gates, operations acting on a fixed number of qubits. Quantum logic gates are a class of operations widely used in quantum computing. They are represented by unitary matrices. The most common quantum gates operate on spaces of one or two qubits, analogous to the common classical logic gates that operate on one or two bits (NIELSEN; CHUANG, 2000).

Another possible choice for the basis is the set $|+\rangle \equiv (|0\rangle + |1\rangle)/\sqrt{2}$ and $|-\rangle \equiv (|0\rangle - |1\rangle)/\sqrt{2}$. The arbitrary state in Eq. 1 can be re-written in this basis as:

$$|\psi\rangle = \frac{\alpha+\beta}{\sqrt{2}}|+\rangle + \frac{\alpha-\beta}{\sqrt{2}}|-\rangle.$$

2.2 DENSITY OPERATOR

As we saw, the state of a quantum system is represented by a state vector $|\psi\rangle$. However, it is possible for a system to be in a statistical ensemble of different state vectors $|\psi\rangle_1, |\psi\rangle_2, ..., |\psi\rangle_n$ with different probabilities $p_1, p_2, ..., p_n$. For this reason the system is often described by a density operator ρ as

$$\rho = \sum_i p_i |\psi_i\rangle\langle\psi_i|, \tag{4}$$

where $p_i \leq 1$ are non-negative real numbers and $\sum_i p_i = 1$. A density operator acting on the Hilbert space $\mathcal{H}$ satisfies:

1. Positivity $\rho \geq 0$, it has a spectral decomposition with only positive eigenvalues:

$$\rho = \sum_j \lambda_j |j\rangle\langle j|; \lambda_j \geq 0,$$

where the states $|j\rangle$ are orthogonal.

2. Hermiticity $\rho = (\rho)^\dagger$.

3. Normalization $\mathrm{Tr}(\rho) = 1$.

A density operator describes a *pure state* if

$$\rho = |\psi\rangle\langle\psi|.$$

In other words, it is a rank one operator, only one eigenvalue is different than zero and equal to 1. In contrast, if ρ cannot be written in this form, the system is in a *mixed state*.

2.3 BLOCH SPHERE

A well known geometrical visualization of a qubit is through the Bloch sphere, named after Felix Bloch, see Fig. 1.

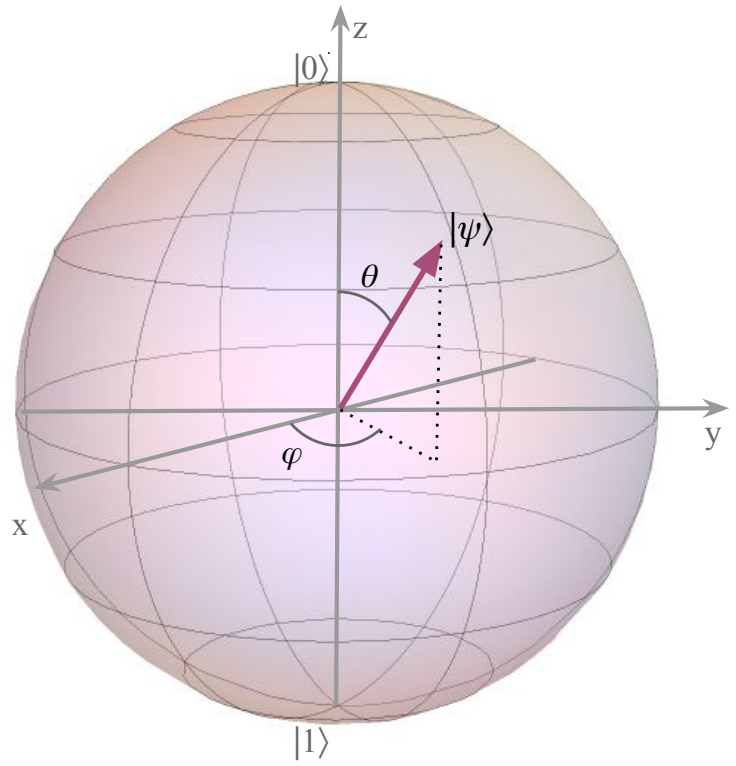

Figure 1 – State of a qubit in the Bloch sphere, parametrized in terms of spherical coordinates.

The Bloch sphere, also called as Bloch ball, is a unit sphere in $\mathbb{R}^3$. The quantum states are uniquely represented by

$$|\psi\rangle = \cos\left(\frac{\theta}{2}\right)|0\rangle + e^{i\phi}\sin\left(\frac{\theta}{2}\right)|1\rangle, \tag{5}$$

where $0 \leq \theta \leq \pi$ and $0 \leq \phi \leq 2\pi$. The parameters θ and ϕ correspond to the spherical coordinates. The states $|0\rangle$ and $|1\rangle$ are at the surface of the sphere and corresponds to the

north pole and south pole, respectively.
Consider $|\chi\rangle$ the opposite point to $|\psi\rangle$ on the Bloch sphere, defined by the spherical coordinates $(1, \pi - \theta, \phi + \pi)$

$$|\chi\rangle = \cos\frac{\pi-\theta}{2}|0\rangle + e^{i(\phi+\pi)}\sin\frac{\pi-\theta}{2}|1\rangle \tag{6}$$

$$= \cos\frac{\pi-\theta}{2}|0\rangle - e^{i\phi}\sin\frac{\pi-\theta}{2}|1\rangle \tag{7}$$

So

$$\langle\chi|\psi\rangle = \cos\frac{\theta}{2}\cos\frac{\pi-\theta}{2} - \sin\frac{\theta}{2}\sin\frac{\pi-\theta}{2}$$

Using $\cos(a+b) = \cos a\cos b - \sin a\sin b$,

$$\langle\chi|\psi\rangle = \cos\frac{\pi}{2} = 0.$$

Opposite points correspond to orthogonal qubit states and this also explains why the angle θ must be divided by 2 in Eq. 5, then two points are orthogonal 90° apart.

A general qubit state can be written as

$$\rho = \frac{1}{2}(\sigma_0 + \sigma_1 r\cos\phi\sin\theta + \sigma_2 r\sin\phi\sin\theta + \sigma_3 r\cos\theta) \tag{8}$$

$$= \sum_i \frac{\mathbb{1} + r_i.\sigma_i}{2}, \tag{9}$$

where σ_i are the well known Pauli matrices σ_x, σ_y and σ_z. The vector $\vec{r} = (r_x, r_y, r_z) = (r\sin\theta\cos\phi, r\sin\theta\sin\phi, r\cos\theta)$ is known as the Bloch vector, with $|\vec{r}| \leq 1$.

A quantum pure state $\rho = |\psi\rangle\langle\psi|$ has $|\vec{r}| = 1$. As a consequence, all pure states are displayed at the surface of the sphere. As previously mentioned, a mixed quantum state is a statistical distribution of pure states, often called a statistical mixture. Contrary to the pure ones, the mixed states remain in the interior of the Bloch ball, $|\vec{r}| < 1$. These notions will be widely used in the next chapters.

We focus our analysis here on qubits and its transformations. As can be seen in the next section, the state space of any finite dimensional quantum system can be understood as a composition of a number of qubits.

2.4 COMPOSITE QUANTUM SYSTEMS

The space state of a larger or composite quantum system is the tensor product of the individual state spaces, for example $\mathcal{H}_{1\ldots n} = \mathcal{H}_1 \otimes \mathcal{H}_2 \otimes \ldots \otimes \mathcal{H}_n$. For two qubits for

example, often called *bipartite systems*, a widely used basis to describe the state is

$$|\Phi^+\rangle = \frac{|00\rangle + |11\rangle}{2}; \tag{10}$$

$$|\Phi^-\rangle = \frac{|00\rangle - |11\rangle}{2}; \tag{11}$$

$$|\Psi^+\rangle = \frac{|01\rangle + |10\rangle}{2}; \tag{12}$$

$$|\Psi^-\rangle = \frac{|01\rangle - |10\rangle}{2}; \tag{13}$$

where $|00\rangle \equiv |0\rangle \otimes |0\rangle$ is a state of two qubits. The above states are called *Bell states*, after John Bell, or sometimes the *EPR states*, after Eistein, Podolski and Rosen pointed out the strange properties of them (EINSTEIN et al., 1935). This strangeness is due to a property called *entanglement*.

Quantum entanglement is related to a strong correlation between parts of a system. For example, a measurement performed in a particle "affects instantly"the particle entangled to it. In 1935, Einstein, Podolski and Rosen argued that no action taken on the first particle could instantaneously affect the other, since this would involve information being transmitted faster than light. A condition forbidden by the theory of relativity (EINSTEIN et al., 1935), that suggests that this sort of relativistic *local causality*, the idea that causal influences should never propagate faster than the speed of light, is a necessary property of any acceptable physical theory. That is why Albert Einstein criticized the quantum mechanics formulation, calling this effect a “spooky action”.

Today we know that there is no such “spooky action”. In fact, quantum mechanics contradicts Einstein’s philosophical postulate that any acceptable physical theory must fulfill "local realism". In 1964, John Bell investigated this situation proposing in (BELL, 1964) a set of inequalities that are just simple probabilistic predictions that must be satisfied by any local realistic theory, but which are violated by correlations in quantum mechanics. He proved that no theory that satisfies the conditions imposed by local realism can reproduce the probabilistic predictions of quantum mechanics under all circumstances. The fact that quantum mechanics violates Bell inequalities indicates that any hidden-variable theory underlying quantum mechanics must be non-local (BELL, 1964).

A composite quantum state ρ_{AB} acting on $\mathcal{H} = \mathcal{H}_A \otimes \mathcal{H}_B$, is called *separable* if it may be written as

$$\rho = \sum_i p_i \rho_A^i \otimes \rho_B^i, \tag{14}$$

with $p_i \geq 0$ and $\sum_i p_i = 1$. Otherwise the state of the system is *entangled*. Another interesting thing widely used in the field of quantum computation is that separable states can be prepared using only local operations, operations performed in each part separately, and classical communication, commonly called LOCC.

If we think of systems with three, four qubits or *multipartite* systems, there are different types of entanglement. Discussions about this can be found in (DÜR et al., 2000).

2.5 DISTINGUISHING QUANTUM STATES

Classically, different states are usually distinguishable, at least in principle. For example, we can always identify the differences between the outcome of an experiment. A simple example is the launch of a coin. It is easy to identify if the coin has landed heads or tails. In the quantum world, is not always possible to distinguish arbitrary states. This indistinguishability of non-orthogonal quantum states is at the heart of quantum computation and quantum information. There are two widely used operational measures that shed a light into this question. These are the *trace distance* and the *fidelity*.

2.5.1 Trace Distance

The trace distance quantifies how close two quantum states are (NIELSEN; CHUANG, 2000; BENGTSSON et al., 2008). Given ρ and σ, the trace distance is defined as

$$D_{tr}(\rho, \sigma) = \frac{1}{2}||\rho - \sigma||_1, \tag{15}$$

where

$$||A||_1 \equiv \mathrm{Tr}\sqrt{A^\dagger A}, \tag{16}$$

is the trace norm. The interpretation of the trace distance is related to the probability of successfully distinguishing the state ρ from σ in a single shot measurement. It can be also understood as a metric on quantum states, with $0 \leq D_{tr} \leq 1$. The trace distance is a particularly good measure of distance between quantum states. Just a simple example, if we take ρ_1 and ρ_2 orthogonal states in the Bloch sphere, this means that $D_{tr}(\rho_1, \rho_2) = 1$.

Another interesting fact is the contractivity property of the trace distance (RUSKAI, 1994) as can be seen below

$$D_{tr}(\Lambda(\rho_1), \Lambda(\rho_2)) \leq D_{tr}(\rho_1, \rho_2), \tag{17}$$

whenever Λ is a trace-preserving quantum operation. The main point here, we will return to it later, is the physical fact that a quantum process acting on two quantum states cannot increase their distinguishability.

2.5.2 Fidelity

Another measure of distance between quantum states is the *fidelity* (JOZSA, 1994). The fidelity is a well known measure of the similarity between two quantum states.

For ρ_1 and ρ_2 density matrices, the fidelity is defined as

$$F(\rho_1, \rho_2) = ||\sqrt{\rho_1}\sqrt{\rho_2}||_1^2. \tag{18}$$

In addition, the fidelity satisfies some interesting and useful properties:

1. $0 \leq F(\rho_1, \rho_2) \leq 1$ and $F(\rho_1, \rho_2) = 1$ iff $\rho_1 = \rho_2$.

2. Is symmetric $F(\rho_1, \rho_2) = F(\rho_2, \rho_1)$.

3. If one of the states is pure $\rho_1 = |\psi\rangle\langle\psi|, F(\rho_1, \rho_2) = \mathrm{Tr}(\rho_1\rho_2)$.

4. (a) It is a convex function. If $\rho_1, \rho_2 \geq 0, p_1 + p_2 = 1$ then

$$F(\rho, p_1\rho_1 + p_2\rho_2) \geq p_1 F(\rho, \rho_1) + p_2 F(\rho, \rho_2)$$

. (b) $F(\rho_1, \rho_2) \geq Tr\rho_1\rho_2$.

5. It is multiplicative, $F(\rho_1 \otimes \rho_2, \rho_3 \otimes \rho_4) = F(\rho_1, \rho_3)F(\rho_2, \rho_4)$.

6. It is non-decreasing after some evolution or any measurement on the states. This means that $F(\rho_1', \rho_2') \geq F(\rho_1, \rho_2)$, where $\rho_1' = \Lambda(\rho_1)$ and $\rho_2' = \Lambda(\rho_2)$. It is also preserved after a unitary evolution.

3 QUANTUM DYNAMICAL MAPS

"Nada é absoluto. Tudo muda, tudo se move, tudo gira, tudo voa e desaparece"

Frida Kahlo

In order to better understand the nature and properties of physical quantum systems, we present in this chapter their evolution over time followed by the mathematical formalism of quantum dynamical maps.

3.1 CLOSED SYSTEMS

In classical mechanics, a closed system is a physical system that does not exchange matter with its surroundings, in thermodynamics is the analogous to an isolated system. There is no heat, work or matter exchange with the reservoir or environment. It is intuitive to notice that in realistic physical systems it is quite difficult to consider that the system is completely isolated from the external influences of the environment. Except if we think at the universe as a whole. The study of closed systems is important to simulate and consequently solve problems in much more complicated systems, even obtaining approximate solutions. In quantum information theory a system is closed if there is no information exchange with the environment. The time evolution can be described by the following first-order linear differential equation (BREUER et al., 2002),

$$\frac{d\rho(t)}{dt} = -\frac{i}{\hbar}[H(t), \rho(t)]. \tag{19}$$

Known as the Liouville-von Neumann equation, where H is the Hamiltonian of the system and contains all information about the interactions driving the dynamics. If the system is closed, states are represented as unit vectors $|\psi\rangle$. Eq. 19 reduces to the well known Schrödinger equation

$$\frac{d|\psi(t)\rangle}{dt} = -\frac{i}{\hbar}H(t)|\psi(t)\rangle. \tag{20}$$

Solving Eq. 19, we obtain :

$$\rho(t) = U(t, t_0)\rho(0)U^{\dagger}(t, t_0), \tag{21}$$

where $U(t, t_0) = e^{-i\int_0^t H(s)ds}$ is the unitary operator governing the evolution, which is subjected to the initial condition: $U(t_0, t_0) = \mathbb{1}$, in other words, the identity operation.

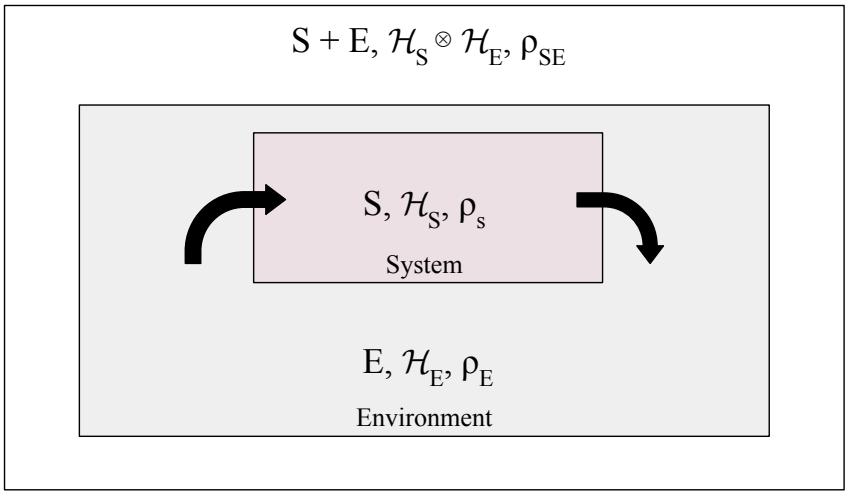

Figure 2 – Schematic representation of an open quantum system.

3.2 OPEN QUANTUM SYSTEMS

In general terms, an open system is a system S coupled to another one E, for which we usually use the term *environment* or even *bath*. The total system is then represented as the combined subsystems $S+E$. Now the subsystem S will change according to its internal dynamics and interaction with the surroundings. Consequently, correlations between S and E could emerge such that the evolution of S can no longer be represented in terms of unitary operators (BREUER et al., 2002). The total Hamiltonian takes now the form

$$H(t) = H_S \otimes \mathbb{1}_E + \mathbb{1}_S \otimes H_E + H_I(t),$$

where H_S is the Hamiltonian of the system S, H_E is the Hamiltonian of the environment and H_I is the Hamiltonian describing the interaction between S and E. A schematic picture is shown in Fig. 2.

As we are interested in the changes at the subsystem S over time, it is possible to obtain the reduced density matrix of the system S as

$$\rho_S = \mathrm{Tr}_E\{\rho_{SE}\}.$$

The equation above represents the partial trace over the degrees of freedom of the environment. From now on, we are looking only for quantities of interest related to S. Since the total density matrix ρ_{SE} evolves unitarily,

$$\rho_S(t) = \mathrm{Tr}_E\{U(t,t_0)\rho_{SE}(t_0)U^\dagger(t,t_0)\}. \tag{22}$$

Analogous to what we observed in Eq. 19, we obtain

$$\frac{d\rho_S(t)}{dt} = -\frac{i}{\hbar}\mathrm{Tr}_E[H(t), \rho(t)].$$

These evolutions can be represented by completely positive and trace preserving (CPTP) maps. Known as quantum operations, superoperators (mathematical definition for an operator acting on another operator) or quantum channels, they will be discussed in further details in this chapter.

3.2.1 Dynamical maps

As we discussed in the previous section, the state of a subsystem S due to its interactions with the environment can change, and its evolution can no longer be represented in terms of a unitary evolution. Regarding the dynamics of the system, we return to Eq. 21. For our purposes, it can be summarized by the following equation

$$\rho_S(t) = \Lambda_{t,t_0}(\rho_S(t_0)), \tag{23}$$

where Λ is a quantum map.

A map is a linear superoperator. In other words, a quantum linear transformation acting on an N-dimensional Hilbert space $\Lambda : \mathcal{H}^{(N)} \to \mathcal{H}^{(N)}$:

$$\rho' = \Lambda(\rho).$$

In order to evolve density operators into density operators, the map must satisfy the following properties: 1.Linearity, 2. Trace preserving, 3. Hermiticity preserving, 4.Positivity (Complete positivity).

Just some considerations regarding the above mentioned properties: 1. Non-linear maps could also map a physical state into another, as can be found in driven-dissipative quantum optical setups. However, with the linearity condition we arrive at more treatable results; 2. and 3. The map preserves the hermiticity and trace of the density matrix; 4. A positive superoperator maps a density matrix into another density matrix. When we move to composite systems, the positivity is no longer sufficient, we require the map to be completely positive.

Since our work consists in analyzing these evolutions, we present the mathematical framework of the dynamical matrix, quite useful to analyze quantum maps.

3.2.1.1 Dynamical Matrix

A quantum map Λ is uniquely characterised by its dynamical matrix. The density matrix ρ of size N can be treated as a vector $\vec{\rho}$ after *reshaping* it (BENGTSSON et al., 2008). We can take as an example

$$\rho = \begin{pmatrix} \rho_{11} & \rho_{12} \\ \rho_{21} & \rho_{22} \end{pmatrix}$$

$$\rightarrow \vec{\rho} = (\rho_{11}, \rho_{12}, \rho_{21}, \rho_{22}).$$

The following formula can also be used

$$\vec{\rho_k} = \rho_{ij} \text{ where } k = (i-1)N + j.$$

Now it is simple to rewrite the equation 23 as

$$\vec{\rho'} = L\vec{\rho} \text{ or } \rho'_{m\mu} = L_{m\mu n\nu}\rho_{n\nu},$$

where L is a linear matrix of size N^2, encoding the transformations of the coordinates of the vector $\vec{\rho}$. It is implicit here the summation over repeated indices.

It is also necessary to present here another operation called *reshuffle*. Given a rectangular $\boldsymbol{X}$ matrix of size $M \times N$. The process of reshuffling consists of reshaping each row of $\boldsymbol{X}$ into a rectangular $M \times N$ submatrix and placing it into a bigger matrix block by block. This gives us

$$X^R_{m\mu n\nu} \equiv X_{mn\mu\nu}.$$

For simplicity, let us take a 4×4 matrix $\boldsymbol{X}$. The correspondent reshuffled matrix can be written as

$$\begin{pmatrix} \boldsymbol{X_{11}} & \boldsymbol{X_{12}} & X_{21} & X_{22} \\ X_{13} & X_{14} & \boldsymbol{X_{23}} & \boldsymbol{X_{24}} \\ \boldsymbol{X_{31}} & \boldsymbol{X_{32}} & X_{41} & X_{42} \\ X_{33} & X_{34} & \boldsymbol{X_{43}} & \boldsymbol{X_{44}} \end{pmatrix}.$$

In bold we observe the elements that remain in the same position as before.

Finally it is possible to introduce D_Λ, the dynamical matrix associated with some evolution Λ :

$$D_\Lambda = L^R. \tag{24}$$

This notion of dynamical matrix was first introduced by Sudarshan in (SUDARSHAN; RAU., 1961). Later these matrices were studied by Choi in (CHOI, 1975). It is common to call them Choi matrices J_Λ:

$$J_\Lambda = (\mathcal{I}_1 \otimes \Lambda_2)|\Omega\rangle\langle\Omega|, \tag{25}$$

where $|\Omega\rangle = \frac{1}{\sqrt{n}} \sum |i\rangle_1 \otimes |i\rangle_2$ is a maximally entangled state. The Choi matrix associated to Λ is the outcome of applying the map on one side of the maximally entangled state. The above representation is also known as *Jamiokolwski isomorphism* (JAMIOŁKOWSKI, 1972). Since it relates a quantum operation Λ to the matrix J_Λ. This isomorphism allows us to treat maps using the same tools as used to treat quantum states.

The most interesting and useful property of this matrix is that it completely determines the map Λ. As can be seen from Eq. 25, if we know somehow how the map acts on $|\Omega\rangle$ we can completely determine how it will act on any other quantum state. The quantum map can also be written as

$$\Lambda(\rho) = \mathrm{Tr}_1\{(\rho^T \otimes \mathcal{I}_2) J_\Lambda\}, \tag{26}$$

where $\mathcal{I}_2$ is the identity map for a qubit, a 2×2 identity matrix. The Choi Matrix approach will be widely explored in Chapters 6 and 7.

3.2.1.2 Positive and completely positive maps

These kind of maps should take density matrices into density matrices. This means that the resulting state ρ' should share the same properties of ρ :

(i) Hermiticity $\rho' = (\rho')^\dagger$.

(ii) $\mathrm{Tr}(\rho') = 1$.

(iii) Positive semi-definite operator $\rightarrow \rho' \geq 0$.

These conditions must been also satisfied by the dynamical matrix J.

(iv) $J_\Lambda = J_\Lambda^\dagger$.

(v) $\mathrm{Tr}_A(J_\Lambda) = \mathcal{I}$.

(vi) $J_\Lambda(\rho) \geq 0$ when $\rho \geq 0$.

Condition (v) shows that the partial trace of J_Λ with respect to the first subsystem is the unity operator for the second subsystem. The condition (vi) requires further explanation. The map is positive if it takes positive matrices to positive matrices. A linear map Λ is positive if and only if the corresponding dynamical matrix is *block positive*.

This condition is not sufficient when we are dealing with physical evolutions. It is common to add an auxiliary system, often called ancillary, to the system of interest.

Consequently the state space is now extended. This requires us to check if the map is still positive in this new configuration. In other words, if $\Lambda \otimes \mathcal{I}$ is positive.

A map is completely positive if and only if for an arbitrary K extension, where $\mathcal{H}_N \to \mathcal{H}_N \otimes \mathcal{H}_K$, the extended map $\Lambda \otimes \mathcal{I}_K$ is positive. This leads us to the following theorem:

Choi's theorem A linear map is completely positive if and only if the corresponding dynamical matrix J_Λ is also positive. A completely positive map can be written in the form

$$\rho \to \rho' = \sum_i K_i \rho K_i^\dagger.$$

This is known as the operator sum representation. The operators K_i are called the Kraus operators. In order to satisfy (ii), the following condition must be satisfied:

$$\sum_i K_i^\dagger K_i = \mathbb{1}.$$

The operator sum is not unique, since it depends on the choice of the basis set. If we had chosen another set we would have arrived to different Kraus operators.

Now, we have all the necessary knowledge to classify a map as completely positive and trace preserving (CPTP). This kind of evolution is widely used and explored in quantum computation and quantum information theory, and also goes under another name: quantum channel.

3.2.2 One-qubit maps

A simple way to deal with CPTP one-qubit maps is using the Bloch sphere representation as presented in Chapter 1. The map of the Eq. 23 can be rewritten as

$$\vec{r}' = \mathbf{T}\vec{r} + \vec{\tau}, \tag{27}$$

where $\mathbf{T}$ is a 3×3 real matrix that, after some orthogonal transformations can be represented in a diagonal form. The elements of these matrices can be represented by the distortion vector $\vec{\eta} = (\eta_x, \eta_y, \eta_z)$ because they take the Bloch ball to an ellipsoid. In other words it determines the shape of the Bloch ball after the action of the map. The vector $\vec{\tau} = (\tau_x, \tau_y, \tau_z)$ is known as a translation vector, because it moves the ellipsoid, and its parameters determine its orientation.

In some cases when $\vec{\tau} = 0$, the maps are classified as *unital*, maps that, when acted on the identity state $\mathbb{1}$, leave it unchanged

$$\Lambda(\mathbb{1}) = \mathbb{1}. \tag{28}$$

The dynamical matrix D_Λ, as presented in Eq. 24, can be written as

$$D_\Lambda = \frac{1}{2}\begin{pmatrix} 1+\eta_z+\tau_z & 0 & \tau_x+i\tau_y & \eta_x+\eta_y \\ 0 & 1-\eta_z+\tau_z & \eta_x-\eta_y & \tau_x+i\tau_y \\ \tau_x-i\tau_y & \eta_x-\eta_y & 1-\eta_z-\tau_z & 0 \\ \eta_x+\eta_y & \tau_x-i\tau_y & 0 & 1+\eta_z-\tau_z \end{pmatrix} \tag{29}$$

The requirement of complete positivity to one qubit quantum channels puts some restrictions on the possible transformations of the Bloch sphere. The map is CP if the ellipsoid remains at the Bloch ball, so an expansion along one of the three orthogonal directions is not allowed, only a contraction. The inverse transformation to a quantum operation is not physical since some mixed states are sent outside the set of positive operators. Some examples of operations in the Bloch ball will be presented in the next section.

3.2.3 Quantum Channels

In this work we analyze typical decoherence quantum channels for a qubit as the dephasing, depolarizing, and amplitude damping channels.

3.2.3.1 Dephasing

The dephasing describes the loss of quantum information, since the coherences, off-diagonal terms of ρ, vanish. Physically it means that the relative phase between the energy eigenstates is lost. The Bloch ball is then contracted to an ellipsoid and the qubits are projected along the z axis as shown in Fig. 3. The map can be written as

$$\Lambda_{deph}(\rho) = \left(1-\frac{p(t)}{2}\right)\rho + \left(\frac{p(t)}{2}\right)\sigma_z\rho\sigma_z, \tag{30}$$

where $p(t)$ is some time dependent probability distribution. The Kraus operators are

$$\boldsymbol{K_0} = \sqrt{1-p(t)}\mathbb{1}$$

,

$$\boldsymbol{K_1} = \sqrt{\frac{p(t)}{2}}\begin{pmatrix} 1 & 0 \\ 0 & -1 \end{pmatrix}$$

After shrinking the sphere, the Bloch vector is $\vec{r'} = (\sqrt{1-p(t)}r_x, \sqrt{1-p(t)}r_y, r_z)$. The states along the z axis remain invariant while the off-diagonal terms decay along time.

3.2.3.2 Depolarizing

In the depolarizing process, with probability $(1-p)$ the system remains intact, while with probability p the the following errors can occur:

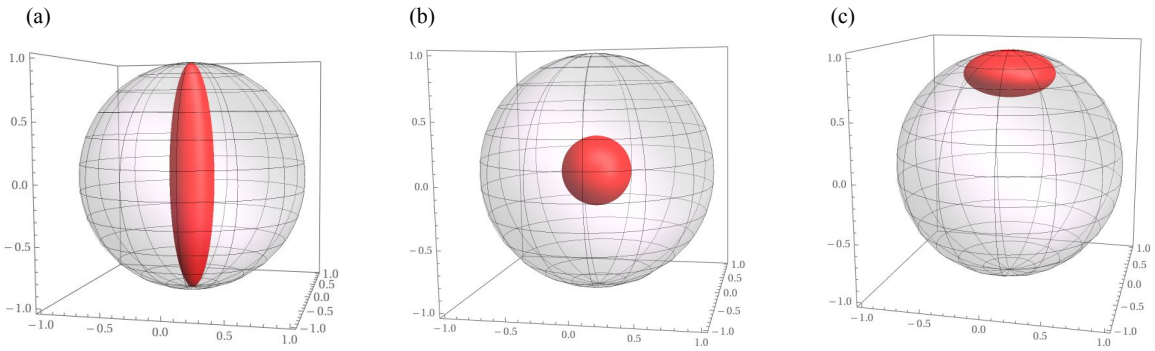

Figure 3 – Action of the quantum channels on the states of the Bloch sphere. In a) dephasing channel schrinking the Bloch ball into an ellipsoid in the z-axis; b) depolarizing taking all states into the maximally mixed state; c) amplitude damping taking all states to the ground state.

1. ***Bit flip*** $: |\psi\rangle \to \sigma_x|\psi\rangle, \sigma_x = \begin{pmatrix} 0 & 1 \\ 1 & 0 \end{pmatrix}$,

2. ***Phase flip*** $: |\psi\rangle \to \sigma_z|\psi\rangle, \sigma_z = \begin{pmatrix} 1 & 0 \\ 0 & -1 \end{pmatrix}$,

3. ***Bit flip + Phase flip*** $: |\psi\rangle \to \sigma_y|\psi\rangle, \sigma_y = \begin{pmatrix} 0 & -i \\ i & 0 \end{pmatrix}$.

It is a channel with nice symmetry properties. As shown in Fig. 3, the Bloch ball is mapped to a sphere with a smaller radius and all the qubits are driven to the maximally mixed state $\mathbb{1}/2$, the center of the Bloch sphere. The channel can be represented as follows

$$\Lambda_{depol}(\rho) = (1 - p(t))\rho + \left(\frac{p(t)}{3}\right)(\sigma_x\rho\sigma_x + \sigma_y\rho\sigma_y + \sigma_z\rho\sigma_z) \tag{31}$$

It is easy to identify the Kraus operators

$$\boldsymbol{K_0} = \sqrt{1 - p(t)}\mathbb{1}, \boldsymbol{K_1} = \sqrt{\frac{p(t)}{3}}\boldsymbol{\sigma_x}, \tag{32}$$

$$\boldsymbol{K_2} = \sqrt{\frac{p(t)}{3}}\boldsymbol{\sigma_y}, \boldsymbol{K_3} = \sqrt{\frac{p(t)}{3}}\boldsymbol{\sigma_z}. \tag{33}$$

After the action of the channel, the resultant Bloch vector is

$$\vec{r'} = (1 - \frac{4}{3}p(t))\vec{r}.$$

This channel can be simply describe as a contraction of the Bloch sphere by the factor $(1 - \frac{4}{3}p(t))$. It is worth mention that it is possible to reverse the action of Λ_{depol} with a inflation. But this is a non-completely positive map, since the inflation will take values of $\vec{r} \leq 1$ to values with $\vec{r} > 1$. Clearly this is not a density operator anymore. The reverse process is then not physical.

3.2.3.3 Amplitude Damping

The amplitude damping channel can be interpreted physically as a two-level system, as the decay of an atom from the excited state due to spontaneous emission of a photon. The ground state is denoted by $|0\rangle$ and the excited state by $|1\rangle$. Transitions may or not occur depending on the state of the system, according to

$$|0\rangle_S|0\rangle_E \rightarrow |0\rangle_S|0\rangle_E$$

$$|1\rangle_S|0\rangle_E \rightarrow \sqrt{1-p(t)}|1\rangle_S|0\rangle_E + \sqrt{p(t)}|0\rangle_S|1\rangle_E$$

The map is represented as

$$\Lambda_{a.d}(\rho) = K_0\rho K_0^\dagger + K_1\rho K_1^\dagger, \tag{34}$$

where the Kraus operators $\boldsymbol{K_0}$ and $\boldsymbol{K_1}$ can be written as

$$\boldsymbol{K_0} = \begin{pmatrix} 1 & 0 \\ 0 & \sqrt{1-p(t)} \end{pmatrix} \qquad \text{and} \qquad \boldsymbol{K_1} = \begin{pmatrix} 0 & \sqrt{p(t)} \\ 0 & 0 \end{pmatrix}. \tag{35}$$

The time dependent decay rate is represented by $p(t)$. After the action of the amplitude damping channel, the entire Bloch ball is contracted to one of the poles of the sphere. All the qubits are driven to the ground state, the north pole of the ball as can be seen in Fig. 3. The resultant Bloch vector is $\vec{r'} = (\sqrt{1-p(t)}r_x, \sqrt{1-p(t)}r_y, p(t) + (1-p(t))r_z)$. This is an example of a non-unital map. It not only compress the sphere, but it also shifts the maximally mixed state to the north pole.

4 NON-BIJECTIVE QUANTUM EVOLUTIONS AND RECOVERING MAPS

"A verdadeira segurança provém apenas do conforto com a insegurança. Ficarmos à vontade com o fluxo das coisas, ficarmos à vontade ao estarmos inseguros, essa é a maior segurança, pois nada pode nos tirar do prumo."

Jetsunma Tenzin Palmo

As mentioned before, non bijective evolutions have been considerably explored (CHRUŚCIŃSKI et al., 2018; JEKNIC-DUGIC et al., 2021). In this chapter we extend the mathematical idea of non-bijective transformations to physical evolutions. Next, we introduce the approach of Petz recovering maps.

4.1 NON-BIJECTIVITY

Bijectivity is a mathematical property from functions and linear transformations. A transformation is bijective if it has a one to one correspondence for all of the elements of the domain. This means that the dimension of the image Im is equal to the dimension of the domain U. Rigorously, the linear transformation $T : U \to V$ is bijective, if for all $v \in V$ there is a unique $u \in U$, such that $T(u) = v$. A non-bijective transformation certainly does not obey this condition. For a non-bijective transformation there is not a one-to-one correspondence, and $dim(Im(U)) < dim(U)$, regarding that $Im(U) \in V$. Consequently these types of transformations do not have a well defined inverse, in other words, they are not invertible. An easy way to visualize it is using diagrams as shown in Fig. 4.

4.1.1 Non-bijective quantum maps

Now we analyze this mathematical property in physical quantum processes. Given a quantum map $\Lambda_{(t_1,0)}$, we wonder if it would be possible to write an evolution capable to reverse the action of the map in time $\Lambda_{(0,t_1)}$, such that

$$\Lambda_{(0,t_1)}\Lambda_{(t_1,0)} = \Lambda^{-1}_{(t_1,0)}\Lambda_{(t_1,0)} = \mathcal{I}$$

Theorem A CPTP map $\Lambda_{(t_1,0)}$ can be inverted by another CPTP map if and only if it is unitary $\Lambda_{(t_1,0)} = U_{(t1,t0)}$ (RIVAS; HUELGA, 2012).

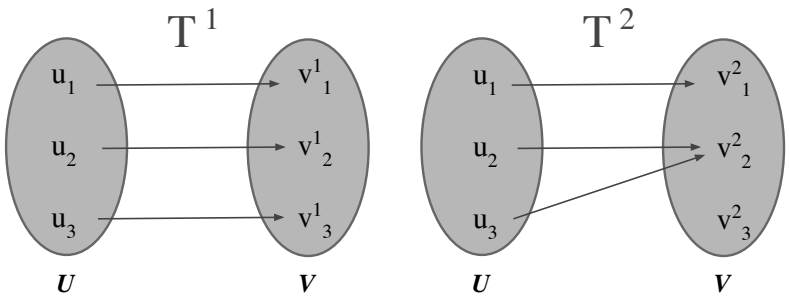

Figure 4 – Diagram of two linear transformations T^1 and T^2, a bijective one and a non-bijetive, respectively. For the first one there is a one-to-one correspondence between the elements of the domain U and V, which corresponds to the image set Im. For the second one, there is not a one-to-one correspondence and the $dim(V) > dim(Im(U))$. In this specific non-bijective case, an inverse $(T^2)^{-1}$ is not well defined, since we can not associate uniquely an element of U to v_2^2.

Mathematically, the inverse of a map can be computed, but in most cases the inverse is not a physical evolution, only if the evolution is unitary.

The main point is that the connection between the failure of an inverse for a dynamical map reflects the irreversibility of the universal open quantum systems dynamics. Regarding the previously mentioned quantum channels, we investigate the limit of non-bijectivity for these CPTP evolutions. To do so, we consider the image non-decreasing condition. Taking the limit of non-bijetivity consists in reducing the image set to its minimum. This is exactly what we will define as follows

(Dephasing) The map drives the states to a line at the z axis that connects the north pole to the south pole and can be represented as

$$\rho_{Im.deph} = q|0\rangle\langle 0| + (1-q)|1\rangle\langle 1|, \tag{36}$$

where q is a probabilistic parameter, which defines what is the state of $\rho' \in Im$.

(Depolarizing) All the states are mapped to the maximally mixed state,

$$\rho_{Im.depol} = \frac{\mathbb{1}}{2} = \frac{|0\rangle\langle 0| + |1\rangle\langle 1|}{2}. \tag{37}$$

(Amplitude Damping) All the states are mapped to the ground state,

$$\rho_{Im.adamp} = |0\rangle\langle 0|. \tag{38}$$

In order to understand the physical implications behind the concept of non-bijectivity in physical quantum systems, we introduce here the approach of recovering maps.

4.2 RECOVERING MAPS

Trying to understand how well it would be possible to reverse a process, the entropic inequalities became a matter of study in recent years. They constitute a fundamental law of quantum information theory, being helpful in determining boundaries and limits to many physical processes.

4.2.1 Quantum Relative Entropy and Uhlmann's Theorem

Classically, given a discrete random variable X, with possible outcomes $\{x_1, ..., x_n\}$, which occur with probability $\{P(x_1), ..., P(x_n)\}$, the entropy of X is formally defined as

$$H(P) \equiv -\sum_{i=1}^{n} P(x_i) \log P(x_i). \tag{39}$$

Where the sum is over all possible values of the variable X. The logarithm is commonly calculated in base 2, which gives the unit of bits. The equation above is known as the Shannon entropy, introduced by Claude Shannon in (SHANNON, 1948). In information theory it is common to relate the idea of entropy with information. Information is directly associated with a "surprisal"of an outcome x_i, which decreases as the probability $P(x_i)$ increases. The entropy in Eq. 39 measures then the average amount of information conveyed by identifying the outcome of a random trial, it is also defined as "uncertainty"and, at the same time, a certain level of "information" about the system (NIELSEN; CHUANG, 2000). Let's return to the example of tossing a coin.

We know that the probability of coming up heads is the same as the probability of tails $P_{heads} = P_{tails} = 1/2$. Of course, there is no such way to predict the outcome of the coin launch ahead of time. Such experiment E has the entropy as high as it could be for a two-outcome trial, $I(E) = 1$. This means that learning the actual outcome contains one bit of information. In contrast, if we use now a coin that has two heads and no tails, there is no information $I(E) = 0$. Since the outcome is always predictable, the coin will always come up heads.

The quantum analogous to the Shannon entropy is the von Neumman entropy (NEUMANN, 1927; NEUMANN, 1933)

$$S(\rho) = -\mathrm{Tr}\rho \log \rho, \tag{40}$$

where ρ is a density operator on a finite dimensional Hilbert space $\mathcal{H}$. The above two equations are related in the following way: if the set X labels an orthonormal basis $\{|x\rangle : x \in X\}$ of $\mathcal{H}$, it is possible to construct

$$\rho_P = \sum_x P(x)|x\rangle\langle x|,$$

corresponding to the distribution $P(x)$. Consequently,

$$S(\rho_P) = H(P).$$

With these definitions in mind, we present now the relative entropy. A function widely used in quantum information theory due to its strong identities and inequalities, providing insights into the quantification of entanglement. The relative entropy also plays an important role in the distinguishability of quantum states. It gives us a picture of a "distance" measure between density operators.

Let ρ and σ be quantum states. We define the quantum relative entropy $S(\rho||\sigma)$ as

$$S(\rho||\sigma) = \mathrm{Tr}\rho\log\rho - \mathrm{Tr}\rho\log\sigma. \tag{41}$$

It has many useful properties (NEUMANN, 1927):

1. $S(\rho||\sigma) \geq 0$, the equality is satisfied if and only if $\rho = \sigma$.

2. $S(\rho||\sigma) < \infty$ if and only if $supp(\rho) \in supp(\sigma)$. The $supp(\rho)$ or support of ρ is the subspace spanned by eigenvectors of ρ with non-zero eigenvalues.

3. The function $S(\rho||\sigma)$ is jointly convex in its arguments. Given $\rho_1, \rho_2, \sigma_1, \sigma_2$ and p_1, p_2 non-negative numbers, such that $p_1 + p_2 = 1$,

$$S(\rho||\sigma) \leq p_1 S(\rho_1||\sigma_1) + p_2 S(\rho_2||\sigma_2),$$

where $\rho = p_1\rho_1 + p_2\rho_2$ and $\sigma = p_1\sigma_1 + p_2\sigma_2$.

Another interesting property of the relative entropy can be seen in (LIEB; RUSKAI, 1973), known as the *monotonicity of the relative entropy*. This property states that discarding part of a composite system AB can only decrease the relative entropy between two density matrices

$$S(\rho_A||\sigma_A) \leq S(\rho_{AB}||\sigma_{AB}).$$

As discussed in the previous section, discarding part of a system can be seen as a quantum operation $T = \mathrm{Tr}_B$, the partial trace over $\mathcal{H}_B$, which as a linear map can be written as $T = \mathcal{I}_A \otimes \mathrm{Tr}$. With this in mind, we finally arrive at the Data Processing Inequality theorem (LIEB; RUSKAI, 1973).

Theorem. Given two quantum states ρ and σ acting on a Hilbert space $\mathcal{H}$, and Λ a quantum channel, the relative entropy between two quantum states does not increase after a CPTP evolution

$$S(\rho||\sigma) \geq S(\Lambda(\rho)||\Lambda(\sigma)). \tag{42}$$

The equality

$$S(\rho||\sigma) = S(\Lambda(\rho)||\Lambda(\sigma)) \tag{43}$$

holds if and only if there is a recovery map $\Lambda_{Recover}$ such that

$$\rho = (\Lambda_{Recover} \circ \Lambda)(\rho), \sigma = (\Lambda_{Recover} \circ \Lambda)(\sigma).$$

The composition of quantum maps $A \circ B$ is a is a mathematical operation analogous to the composition of two functions $f \circ g$. It is worth mentioning that the composition of two completely positive maps yields again a completely positive map (BENGTSSON et al., 2008).

In this work we will explore a type of recovery map known as the Petz recovery map Λ_{Petz}.

4.2.2 Petz recovery maps

The Petz recovery map, developed initially by Dénes Petz in (PETZ, 1986; PETZ, 1988) and further analyzed in (PETZ, 2003; AL., 2018), is a completely positive, trace preserving and unique on the support of $\Lambda(\sigma)$. For finite Hilbert spaces, on the support of $\Lambda(\sigma)$, the Petz can be written as

$$\Lambda_{Petz}(.) = \sigma^{\frac{1}{2}}\Lambda^{\dagger}(\Lambda(\sigma)^{-\frac{1}{2}}(.)\Lambda(\sigma)^{-\frac{1}{2}})\sigma^{\frac{1}{2}} \tag{44}$$

where Λ is the evolution that we are trying to reverse and σ is known as the reference state of the map such that

$$supp(\rho) \in supp(\sigma). \tag{45}$$

Furthermore, the adjoint map $\Lambda^{\dagger}$ of Λ can be written as

$$\Lambda^{\dagger}(\rho) = \sum_i A_i^{\dagger}\rho A_i \text{ if } \Lambda(\alpha) = \sum_i A_i \alpha A_i^{\dagger}, \tag{46}$$

where α is a quantum state. The existence of an explicit recovery map is universal in the sense that it depends only on the reference state σ and the quantum channel Λ to be reversed (AL., 2018). From Eq. 44, it is possible to show the following properties of the Petz recovery map:

i) It is linear, completely positive and trace preserving

$$\begin{aligned}
\mathrm{Tr}\{\Lambda_{Petz}(\rho)\} &= \mathrm{Tr}\{\sigma^{\frac{1}{2}}\Lambda^{\dagger}(\Lambda(\sigma)^{-\frac{1}{2}}\rho\Lambda(\sigma)^{-\frac{1}{2}})\sigma^{\frac{1}{2}}\} \\
&= \mathrm{Tr}\{\sigma\Lambda^{\dagger}(\Lambda(\sigma)^{-\frac{1}{2}}\rho\Lambda(\sigma)^{-\frac{1}{2}})\} \\
&= \mathrm{Tr}\{\Lambda(\sigma)(\Lambda(\sigma))^{-\frac{1}{2}}\rho(\Lambda(\sigma))^{-\frac{1}{2}}\} \\
&= \mathrm{Tr}\{\rho\}
\end{aligned}$$

ii) Perfectly recovers σ from $\Lambda(\sigma)$

$$\begin{aligned}\Lambda_{Petz}(\Lambda(\sigma)) &= \sigma^{\frac{1}{2}}\Lambda^{\dagger}(\Lambda(\sigma)^{-\frac{1}{2}}\Lambda(\sigma)\Lambda(\sigma)^{-\frac{1}{2}})\sigma^{\frac{1}{2}} \\ &= \sigma^{\frac{1}{2}}\Lambda^{\dagger}(\mathbb{1})\sigma^{\frac{1}{2}} \\ &= \sigma\end{aligned}$$

This is an interesting property, because it give us a hint about the reference state σ. Observe that it is always a recoverable state for the Petz. This can be easily understood because the recovery map has some amount of information about σ in its form, see Eq. 44. In the following chapter the dependence of the success of the Petz recovering states with the reference state will become clearer.

iii) If the evolution to be reversed is the identity map $\Lambda = \mathcal{I}$, the Petz is the identity map

$$\Lambda_{Petz} = \mathcal{I}.$$

This condition is quite intuitive, because, if nothing happens, nothing changes the state, and consequently there is no need to recover some information.

For the two following properties we define $\Lambda_{Petz} \equiv \Lambda^{\sigma,\Lambda}_{Petz}$, the recovery map associated with the channel Λ and the reference state σ.

iv) Tensor products The Petz recovery map is a tensor product of individual Petz recovery maps:

$$\Lambda^{\sigma_1\otimes\sigma_2,\Lambda_1\otimes\Lambda_2}_{Petz} = \Lambda^{\sigma_1,\Lambda_1}_{Petz} \otimes \Lambda^{\sigma_2,\Lambda_2}_{Petz}$$

v) Composition of channels $\Lambda_1 \circ \Lambda_2$

$$\Lambda^{\sigma,\Lambda_1\circ\Lambda_2}_{Petz} = \Lambda^{\sigma,\Lambda_1}_{Petz} \circ \Lambda^{\Lambda_1(\sigma),\Lambda_2}_{Petz}$$

It seems a little bit complicated, but observe that, in order to achieve a pretty good recovery, it is necessary first to recover from the last noise, when even the reference state was affected $\Lambda_1(\sigma)$, and than recover from the first noise.

The last three conditions can be found in (LI K., 2018). The whole mathematical framework of this approach was developed by Petz in (PETZ, 1986; PETZ, 1988; PETZ, 2003).

5 INVERTING NON-BIJECTIVE EVOLUTIONS THROUGH RECOVERING CHANNELS

"Imaginação é quando a inteligência se diverte"

Rita Lee

Using the approach of Petz recovering maps described in the previous section, we propose to construct an inverse evolution in the limit of non-bijectivity to the mentioned one qubit quantum channels, as dephasing, depolarizing and amplitude damping. In this chapter we present in the first section, our approach to reverse the dynamics, in the second section the obtained results, and in third section we analyze and discuss the implications of this work.

5.1 COMPUTING THE INVERSE

To construct a physical inverse evolution, we set a simple quantum circuit as shown in Fig. 5. The gates Λ and Λ_{Petz} are the quantum channels and the Petz recovery map, respectively.

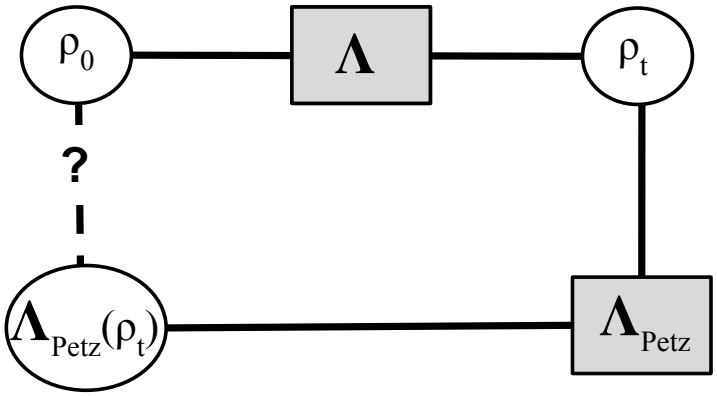

Figure 5 – Schematic representation of the total evolution including the Petz recovery map. A initial state ρ_0 is taken to a evolved state $\rho_t = \Lambda(\rho_0)$. The Petz is then applied to the evolved state $\Lambda_{Petz}(\rho_t)$.

The main idea is to compare the state recovered by the Petz map $\Lambda_{Petz}(\rho_t)$ to the initial state ρ_0 that we had before the evolution. With the results in hand it will then be possible to consider and analyze all variables, in order to build an inverse operation whose outcome is as close as possible to ρ_0.

To do this comparision between $\Lambda_{Petz}(\rho_t)$ and ρ_0, we use the *fidelity* as the figure of merit. Its properties were presented in Section 2.5.

5.2 RESULTS

Based on what we developed in the previous sections, we present in this section the results obtained by this analysis.

5.2.1 Behavior of the fidelity according to the Petz

In order to understand the Petz behavior and consequently its efficiency in recovering a previously lost information, we begin our analysis by observing the behavior of the fidelity function, $F(\rho_0, \Lambda_{Petz}(\rho_t))$ for each one of the evolutions. For this analysis, the parameter t is fixed since the quantum channels were set at the regime of non-bijectivity, as presented in Section 4.1.1. It is worth to mention here, that for the amplitude damping channel we took the closest value to one, approximately $p(t) = 0.99$. There is no difference if we set, for example, $p(t) = 0.999$ or $p(t) = 0.9999$. The evolution is not sensible to this minimal changes. Although the theoretical limit was defined in Section 4.1.1, this approximation is necessary for the amplitude damping channel, because if we look at Eq. 44, the map diverges for $p(t) = 1$, since the inverse of $\sigma = |0\rangle\langle 0|$ cannot be calculated numerically.

In Fig. 6 below, we observe the maximal dephasing, depolarizing and amplitude damping acting on pure states $\rho_0(\theta, \phi)$. It is possible to note the strong dependence of the Petz *efficiency*, here to be considered as the capacity of recovering the state, represented by the fidelity function, with the previously fixed reference state σ.

From Fig. 6 it is easy to see that when we are trying to recover states close to the chosen reference state, the value of the fidelity is high and consequently the efficiency is high. On the contrary, if the state to be recovered is far from the reference state, the fidelity decays a lot. Since there is this sense of proximity, it is not possible to find a Petz recovery map that works equally well for all states of the Bloch sphere. Here we arrive at an interesting point of this analysis, the emergence of certain domains or regions were a recovery map reaches its biggest values of fidelity. Therefore we found quantum states that can always be recovered. We will return to this point later.

To summarize, the Petz works really well depending on the choice of σ. At the beginning it seems complicated to identify which reference state fits best for our pourposes. As the name *reference* says, we can interpret σ as some amount of information that we have about the initial state ρ_0. In a more realistic scenario, when we are dealing with uncontrollable parameters and environments, we do not have this information and that is the reason why this work can be useful to some extent. The main point here is to build a recovery map capable to recover the initial state without having any previous information about the ρ_0. At this point I consider that the analogy from Fig. 7 can be very useful to

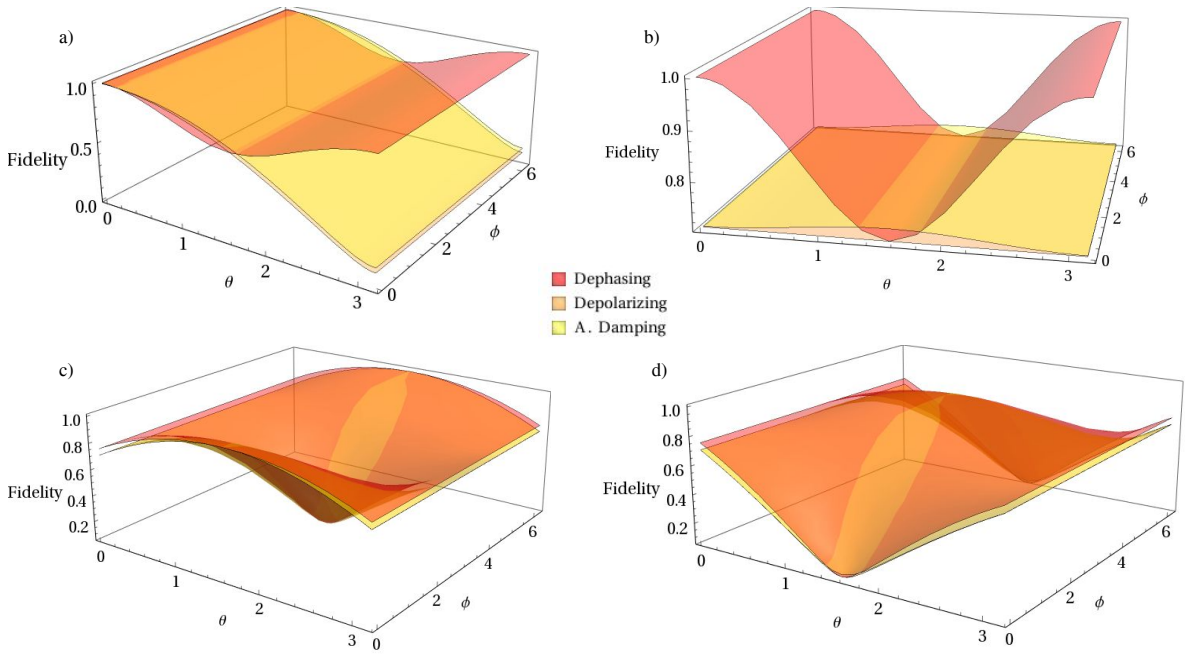

Figure 6 – Fidelity of the state recovered by the Petz $\Lambda_{Petz}(\rho_t)$ and initial pure states $\rho_0(\theta, \phi)$ parametrized in terms of the spherical coordinates, θ and ϕ. In a) with σ fixed next to $|0\rangle\langle 0|$ the fidelity is high for ρ_0 next to it but decays as we move away from this point. The same is not observed for the dephasing, which increases from $\theta \in [\pi/2, \pi]$. In b) $\sigma = \mathbb{1}/2$, we observe the same behavior for the dephasing but for the other two evolutions, the fidelity remains constant at approximately 0.7. c) $\sigma \approx |+\rangle\langle +|$ that obtain high values for states next to it, and it is also possible to notice the decay of the fidelity when we approach the orthogonal state $|-\rangle\langle -|$. d) $\sigma \approx |-\rangle\langle -|$ we observe the exact opposite to c).

clarify this point.

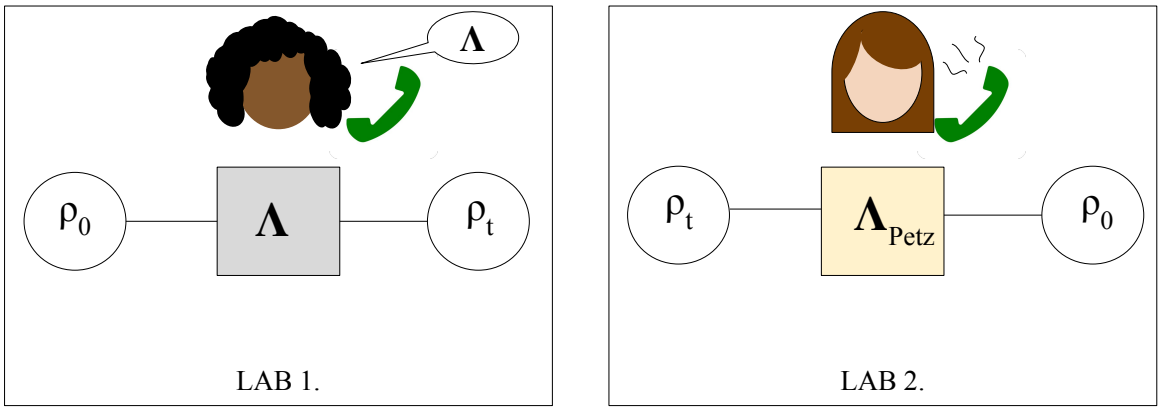

Figure 7 – Example of an experiment reproducing the construction of the Petz recovery map. Observe that this is an ideal scenario where no information about the state to be recovered ρ_0 was provided.

Suppose that in the Lab 1 a person evolves a initial state ρ_0 through some quantum channel Λ to a final state ρ_t. Then, this experimentalist communicates the performed process to a friend in another laboratory, Lab 2. The friend from Lab 2 does not have any

information about the initial state ρ_0 but since she knows the process Λ, she is capable to build a recovery map that recovers ρ_0 no matter which evolved state ρ_t she receives.

Based on Fig. 6, we noticed that it is not easy to build an inverse evolution completely "blindly". For this reason, in order to analyze the efficient recovery map for this scenario, or at least clarify which way can be taken, we propose in the following subsection the best strategy independent of the initial state.

5.2.2 Best recovery map for each one of the evolutions

We developed a numerical simulation to find the best sigma σ_{best} that maximizes the value of the fidelity for each one of the evolutions. The algorithm is quite simple. We generate a random mixed reference state σ, specified in the Appendix A, and calculate the fidelity between the state recovered by the Petz and the initial state $F(\Lambda_{Petz}(\Lambda(\rho_0)), \rho_0)$. We obtained a set of pairs $(\sigma_0, \bar{F}_0), (\sigma_1, \bar{F}_1), ..., (\sigma_n, \bar{F}_n)$, where $\bar{F}_i = \sum_\alpha^n F(\rho_\alpha, \Lambda_{Petz}(\rho_{\alpha_t}))/n$ is the fidelity on average for n initial randomly chosen states, using the reference state σ_i. For each reference state we took an average of the fidelity over $n = 10^4$ initial states (this number will be specified in the Appendix B). After that, we pick the best pair which corresponds to the highest fidelity on average and the correspondent recovery map. The obtained values for the fidelity were $\bar{F} = 0.8623$ for the dephasing, $\bar{F} = 0.7951$ for the depolarizing and $\bar{F} = 0.8094$ for the amplitude damping map.

The results are quite interesting. Proving our assumption from the beginning, the maximally mixed state seems to be a good choice for σ. It is a state that satisfies the condition in Eq. 45 and if we are analyzing the whole state space for a qubit, it is reasonable that the central point of the sphere is a good reference state on average.

The above result, specifically the different numerical values of $\bar{F}$, is also directly related to the image set on the limit of non-bijectivity in Eqs. 36-38 for the dephasing, depolarizing and amplitude damping map, respectively. The image state plays an important role in the study of evolutions. It is intuitive to classify these points as some amount of information about the process. Since they are states that never change over time. It is worth to mention that for the dephasing channel, as can be seen in Eq. 36, the image state is actually a set of states. Confirming our analysis, we noticed that any state of this set satisfies the condition as the best σ on average.

5.2.2.1 Hierarchy between quantum channels

To clarify this point, Fig. 8 shows the fidelity function behavior in terms of initial mixed states $\rho_0 = \rho_0(r, \theta, \phi)$. At the beginning we were looking only for pure states $\rho_0 = \rho_0(1, \theta, \phi)$, but now the analysis was extended for the whole Bloch sphere. Due

to symmetry properties of the mentioned quantum channels, the azhimutal angle was fixed, without loss of generality, to $\phi = 0$. Following the r axis in Fig. 8 a) the value of $F(\rho_0, \Lambda_{Petz}(\rho_t))$ begins in its maximum and decreases as long as ρ_0 reaches pure states ($r = 1$) for all the three quantum channels. In Fig. 8 b) we observe another view of the same image where it is possible to note that the initial state is better recovered for the dephasing channel in comparison to the other evolutions, since the fidelity maintains itself more stable at its maximum.

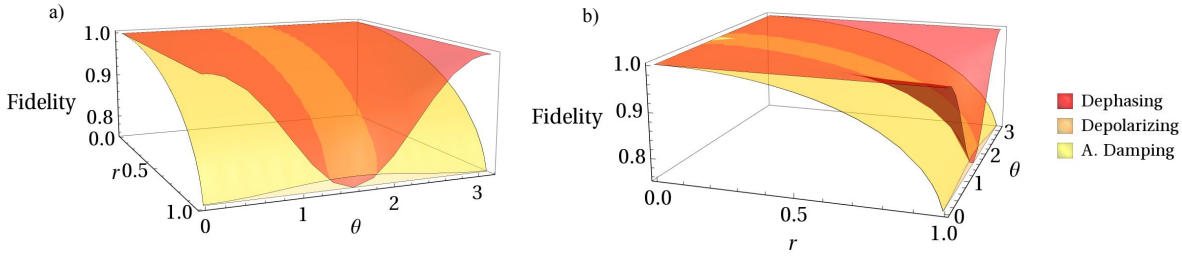

Figure 8 – Plot of the fidelity in terms of initial mixed states for both three evolutions. The Petz recovery map was previously prepared with $\sigma = \mathbb{1}/2$ for each channel. In a) a frontal view, in b) a side view where it is possible to see the different behavior for the dephasing map.

With the above results in hand, we propose a hierarchy for the quantum channels characterized by the non-invertibility degree of the maps. A connection between the results obtained using the Petz approach and the invertibility of the channels can be easily made, if we think about the image state defined in section 4.1.1.

As already mentioned, the dephasing channel presents higher values for the fidelity compared to depolarizing and amplitude damping, which have values so close to each other, in a manner that the channels cannot be distinguished in Fig. 8, since the curves are overlapped. Now the question is what differs the dephasing from the other evolutions? Based on what was developed in this work, the answer is quite simple to understand. The image set of this quantum channel, at the limit of non-bijectivity, corresponds to a line that contains an infinite number of states that can be the best state on average. From another perspective, after a totally dephasing evolution we lose less information than for a totally depolarizing one, for example, where all the initial states converge to the maximally mixed state. The key point is that, *the harder it is to retrieve information from a channel, the more non-invertible it can be classified.*

It must be taken into account, of course, that the image set depends on the domain where the map is acting. In this work our analysis was more general, since we were looking for the whole Bloch sphere, the subspace of all one-qubit states, where no constraints or bounds were imposed. However, we saw that depending on what σ the experimentalist

chooses, the Petz recovery map achieves different performances. The same can happen if there are constraints on the space where the map Λ is acting, for example a mini-ball inside the Bloch sphere positioned more to the left of the center. Or, another case, if there is a non-uniform distribution of states at the sphere, with all of them positioned only in the north hemisphere or only in the south hemisphere. For sure, the best reference state, consequently the best recovery map, will change for each one of these situations. Yet our proposed analysis can be helpful.

5.2.3 Without applying the recovery map

This section consists in comparing the Petz recovery map to an identity channel. Basically we want to see if our strategy works well compared to simply not doing it. In other words, we would like to analyze how good the Petz is to recover the initial state compared to the strategy were no recovering is performed. The identity channel is defined as

$$\mathcal{I}(\rho) = \rho.$$

A schematic idea is shown in Fig. 9.

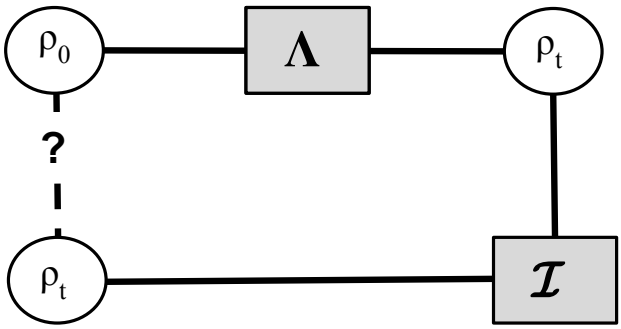

Figure 9 – The final state is simply the state after the evolution $\rho_f = \Lambda(\rho_0) = \mathcal{I}\Lambda(\rho_0)$.

We calculated the fidelity between the initial state ρ_0 and the evolved one ρ_t, $F(\rho_0, \rho_t)$. The obtained results are $\bar{F}_{identity} = 0.8610$ for the dephasing, $\bar{F}_{identity} = 0.7945$ for the depolarizing, and $\bar{F}_{identity} = 0.4971$ for the amplitude damping map. Quite similar to the results using the Petz recovery map in the Section 5.2.2, at least for the dephasing and depolarizing channels.

This can be analytically verified if we consider σ as the best reference state on average in the Eq. 44. Replacing σ by $\mathbb{1}/2$, since both channels are unital maps, as explained in Chapter 3, Eq. 28, we observe that the Petz in Eq. 44 reduces to the map Λ itself. In other words, the map is moving the input state ρ_t to the opposite direction of the initial state ρ_0. Thinking of an invertibility perspective, the state is pushed away from the backward direction. Of course the Petz strategy works, but since the identity channel

give us less work, it should be preferable to use it. The calculations of this strategy can be seen in Appendix C.

The same is not observed for the amplitude damping channel, a non-unital map. The Petz performance is twice as good as the performance of the identity channel. This can be confirmed analytically replacing σ and testing different input states. It is not clear if there is something else behind the invertibility of unital and non-unital maps. At least not from the Petz perspective yet.

It is worth mentioning that the previous results are for one-qubit channels, as one-qubit identity channel, and the same for the fidelity measure. As shown in Eq. 44, the Petz is a general map which can be extended for higher dimensions. Repeating this analysis may have a different result for higher dimensions.

6 ANALYZING NON-MARKOVIAN EVOLUTIONS

"In my opinion, a problem is something that takes your life off the tracks - an inconvenience is not being able to sit in your favorite seat on the runaway train in question"

Carrie Fisher (Princess Leia)

In this chapter we review the concept of classical Markov processes and then adapt it to the quantum case. Later we characterize non-Markovianity, introducing some useful measures to its quantification and witnessing in quantum systems.

6.1 MARKOVIAN EVOLUTIONS

Classically, a stochastic process is a family of random variables X depending on time. It is called as a *Markovian* process if the probability that a random variable X takes the value x_n at any time t_n depends only on the value x_{n-1} that it took at the time t_{n-1}. In other words, a Markov process does not have memory of the past values of the variable X. This can be represented in terms of the conditional probabilities

$$p(x_n, t_n|x_{n-1}, t_{n-1}; ...; x_0, t_0) = p(x_n, t_n|x_{n-1}), \forall t_n \in I,$$

where I is some time interval. Markov processes, named after the Russian mathematician A. Markov, are defined in terms of the Chapman-Kolmogorov equation (BREUER et al., 2002):

$$p(x_3, t_3|x_1, t_1) = \int dx_2 p(x_3, t_3|x_2, t_2)p(x_2, t_2|x_1, t_1). \tag{47}$$

This equation says that the probability of going from state 1 to state 3 can be found from the probabilities of going from 1 to an intermediate state 2 and then from 2 to 3, by adding up over all the possible intermediate states 2. In the quantum case, the classical Chapman-Kolmogorov equation is replaced by

$$\Lambda_{(t_2,t_0)} = \Lambda_{(t_2,t_1)}\Lambda_{(t_1,t_0)}, \text{ for } t_2 \geq t_1 \geq t_0. \tag{48}$$

The equation above defines the *divisibility* property. As we saw in Chapter 3, an operation describing the evolution of a system over time is called dynamical map. If the map can be expressed as a sequence of linear maps, as in Eq. 48, it is called divisible.

Definition. A quantum system under the action of a family of trace preserving linear maps $\Lambda_{(t_2,t_1)}$, where $t_2 \geq t_1$, is Markovian if for every t_2 and t_1, $\Lambda_{(t_2,t_1)}$ is a complete positive map and satisfies Eq. 48.

A very nice property of the divisibility condition is that it may be defined without any explicit mention to measurement processes. In quantum systems this is a huge advantage since a measurement can change and disturb the state of the system. It is also possible to obtain a differential equation for $\rho(t)$, called the *Master equation* (BREUER et al., 2002).

We know by definition that the derivative corresponds to the following limit for $\epsilon \to 0$:

$$\frac{d\rho(t)}{dt} = \lim_{\epsilon \to 0} \frac{\rho(t+\epsilon) - \rho(t)}{\epsilon}. \tag{49}$$

Consider the difference

$$\rho(t+\epsilon) - \rho(t) = [\Lambda_{(t+\epsilon,0)} - \Lambda_{(t,0)}]\rho(0) = [\Lambda_{(t+\epsilon,t)} - \mathbb{1}]\Lambda_{(t,0)}[\rho(0)] = [\Lambda_{(t+\epsilon,t)} - \mathbb{1}]\rho(t).$$

Now, substituting the expression above in Eq. 49, we obtain

$$\frac{d\rho(t)}{dt} = \lim_{\epsilon \to 0} \frac{[\Lambda_{(t+\epsilon,t)} - \mathbb{1}]}{\epsilon}\rho(t) = \mathcal{L}_t\rho(t), \tag{50}$$

where $\mathcal{L}_t$ is known as the *generator* of the evolution. If the evolution is Markovian, we arrive at the following result.

Theorem. An operator $\mathcal{L}_t$ is the generator of a Markovian process if and only if it can be written as

$$\frac{d\rho(t)}{dt} = \mathcal{L}_t[\rho(t)] = \frac{-i}{\hbar}[H(t), \rho(t)] + \sum_k \gamma_k(t)[V_k(t)\rho(t)V_k^\dagger(t) - \frac{1}{2}V_k^\dagger(t)V_k(t), \rho(t)], \tag{51}$$

the famous Gorini-Kossakowski-Susarshan-Lindblad (GKSL) (LINDBLAD, 1976; GORINI et al., 1976) equation, where $H(t)$ is the self-adjoint Hamiltonian that determines the system dynamics, $V_k(t)$ is a time dependent operator, and $\gamma_k(t) \geq 0$ ensure that the equation is trace-preserving and complete positive. If the dissipation rate $\gamma_k(t)$ is zero, then the equation above reduces to the quantum Liouville equation for a closed system, as shown in Eq. 19, also known as the von Neumann equation. The GKSL master equation describes the evolution of an open quantum system in the weak-coupling limit. Further assumptions have to be made, known as Born-Markov approximations:

1. Slowly developing of the correlations between system and environment.
2. Excitations of the environment decay quickly.
3. When compared to the system timescale, terms that oscillate fast can be neglected.

It is easy to understand that in realistic physical systems, the assumption of a Markovian dynamics relies in simplifications that neglect all memory effects to describe the system.

The phenomenon of the non-trivial memory effects in open quantum systems, known as the non-Markovian regime, has been extensively investigated in recent years. A large variety of analytical and numerical methods were developed to quantify the degree of non-Markovianity in physical systems, as can be seen in (RIVAS et al., 2014; VEGA; ALONSO, 2017; LI et al., 2020; LI et al., 2019).

6.2 NON-MARKOVIAN RANDOM UNITARY QUBIT DYNAMICS

In this section we present the analysis developed in (CHRUŚCIŃSKI; WUDARSKI, 2013), which is quite useful for our purposes, as will be seen in Chapter 7.

A random unitary dynamical map can be described by

$$\Lambda_t \rho = \sum_{\alpha=0}^{3} p_\alpha(t) \sigma_\alpha \rho \sigma_\alpha, \tag{52}$$

where σ_α are the Pauli matrices and $p_\alpha(t)$ is a time-dependent probability distribution, such that $p_0(0) = 1$ guarantees $\Lambda_0 = \mathbb{1}$. Aiming to build a non-Markovian evolution Λ_t, we must find a local generator $\mathcal{L}_t$ that does not satisfy the GKLS theorem presented in Section 6.1. Based on the results from (CHRUŚCIŃSKI; WUDARSKI, 2013), the local generator is given by

$$\mathcal{L}_t(\rho) = \sum_{k=1}^{3} \gamma_k(t)(\sigma_k \rho \sigma_k - \rho). \tag{53}$$

As previously discussed, the dissipation rates γ_k are time dependent functions which must be positive to satisfy the Markovianity condition.

Definition. The random unitary dynamics in Eq. 52 is Markovian if and only if,

$$\gamma_1(t) \geq 0, \gamma_2(t) \geq 0, \gamma_3(t) \geq 0, \text{ for all } t \geq 0. \tag{54}$$

The time dependent probabilities shown in Eq. 52, and also in Eqs. 30-34 are characterized in terms of these decay rates $\gamma_{i's}(t)$.

Let us introduce

$$\Gamma_k(t) = \int_0^t \gamma_k(\tau)d\tau. \tag{55}$$

The probability distributions $p_\alpha(t)$ are given by

$$p_0(t) = \frac{1}{4}[1 + A_{12}(t) + A_{13}(t) + A_{23}(t)],$$

$$p_1(t) = \frac{1}{4}[1 - A_{12}(t) - A_{13}(t) + A_{23}(t)],$$

$$p_2(t) = \frac{1}{4}[1 - A_{12}(t) + A_{13}(t) - A_{23}(t)],$$

$$p_3(t) = \frac{1}{4}[1 + A_{12}(t) - A_{13}(t) - A_{23}(t)],$$

where $A_{ij}(t) = e^{-2[\Gamma_i(t)+\Gamma_j(t)]}$. For a deduction and more detailed algebraic calculations, see (CHRUŚCIŃSKI; WUDARSKI, 2013).

We can choose then negative rates and the correspondent probabilities to construct a wide range of non-Markovian evolutions for one-qubit dynamics.

6.3 MEASURING AND WITNESSING QUANTUM NON-MARKOVIANITY

After introducing the theoretical aspects and presenting examples of quantum non-Markovian systems, we may think about its quantification and detection. We begin by presenting some useful techniques to quantify and witness non-Markovianity in quantum systems as geometric mesures, RHP measure and the BLP quantifier. A good question we may ask ourselves is about the difference between those techniques. Basically a measure is more related to *quantification*, for example, a function which assigns a number to each dynamics. Such number can be seen as a markovianity (non-markovianity) degree. A witness is related to *detection*, whose outcomes are "yes" or "no".

6.3.1 Geometric measure

This measure is expressed as a distance between some dynamical map $\Lambda_{t,0}$ and its closest Markovian dynamics $\Lambda^M_{t,0}$, originally proposed in (WOLF; CIRAC, 2008). The quantity $\mathcal{D}(\Lambda_1, \Lambda_2) \in [0, 1]$ is some distance measure in the space of dynamical maps. The geometric non-Markovianity measure for some time t is then defined as

$$\mathcal{N}_t^{geo}[\Lambda_{(t,0)}] := \min_{\Lambda^M \in \mathcal{M}} \mathcal{D}(\Lambda_{t,0}, \Lambda^M_{t,0}),$$

where $\mathcal{M}$ is the set of Markovian dynamics. Observe that this value is zero if and only if $\Lambda_{t,0}$ belongs to the set $\mathcal{M}$. The geometric measure of non-Markovianity in some time interval I is the maximum value of the geometric non-Markovianity for $t \in I$,

$$\mathcal{D}^I_{NM} := \max_{t \in I} \mathcal{N}_t^{geo}[\Lambda_{t,0}]. \tag{56}$$

This quantity can be seen as a degree of non-Markovianity whose values lie between 0 and 1 and is positive if an only if the process is non-Markovian. Despite the measure being very easy to understand, it is quite difficult to be computed, since it involves an optimization process.

6.3.2 RHP measure

Another widely used measure was proposed by Rivas, Huelga and Plenio (RIVAS et al., 2010; RIVAS et al., 2014). The RHP measure is worth to be mentioned because it is much simpler to be computed than the previous one, since it does not involve an optimization. Given a family $\Lambda_{t_2,t_0}, t_2 \geq t_0$, the idea is to quantify the positiveness of the intermediate dynamics $\Lambda_{t_2,t_1}, t_2 \geq t_1$, for every time t_1.

Regarding the Eq. 48, we know that for non-Markovian dynamics, there must be some t_1, such that Λ_{t_2,t_1} is not CP. To quantify how much the intermediate map is NCP, they used the Choi-Jamiolkowski isomorphism, presented in Chapter 3.

The Choi Matrix related to this evolution can be calculated as shown below:

$$[\Lambda_{t_2,t_1} \otimes \mathbb{1}](|\Phi\rangle\langle\Phi|), \tag{57}$$

where $|\Phi\rangle$ is a Bell state. The map is CP if and only if the Choi matrix is positive semidefinite. The trace norm of this matrix, discussed in Section 2.5, provides a measure of the NCP character of Λ_{t_2,t_1}:

$$||[\Lambda_{t_2,t_1} \otimes \mathbb{1}](|\Phi\rangle\langle\Phi|)||_1 \begin{cases} = 1, \text{iff is CP}, \\ > 1, \text{otherwise}. \end{cases} \tag{58}$$

Now it is possible to define a function $g(t)$ that is the right derivative of the trace norm:

$$g(t) := lim_{\epsilon \to 0^+} \frac{[\Lambda_{t_2,t_1} \otimes \mathbb{1}](|\Phi\rangle\langle\Phi|) - 1}{\epsilon} \tag{59}$$

So, if $g(t) > 0$ for some t, the evolution is non-Markovian. The total amount of non-Markovianity in an interval $t \in I$ will be given by

$$\mathcal{N}_{RHP}^{I} := \int_I g(t)\, dt. \tag{60}$$

To compute this measure it must be taken into account that it is necessary to know the complete dynamics to compute the function $g(t)$.

6.3.3 BLP quantifier

Based on the trace distance $D_{tr}(\rho_1, \rho_2)$ for two quantum states ρ_1 and ρ_2, Breuer, Laine and Piilo define the rate of change of the trace distance as

$$\sigma(\rho_1, \rho_2, t) := \frac{dD_{tr}[\rho_1(t), \rho_2(t)]}{dt}.$$

As proved in (RUSKAI, 1994), all CPTP maps are contractions for the trace distance. This means that no trace preserving quantum operation can ever increase the distinguishability of two states. As demonstrated in (BREUER et al., 2009), $\sigma(\rho_1, \rho_2, t) \leq 0$ for Markovian processes. There are, however, physical processes where this quantity is larger than zero for certain times. Processes which we call non-Markovian.

In order to construct a quantity to measure the total increase of distinguishability over the whole time-evolution, let us say for some time interval I, they introduce the BLP measure as follows

$$\mathcal{N}_{BLP} := \max_{\rho_1,\rho_2} \int_{\sigma>0} \sigma(\rho_1, \rho_2, t)\, dt. \tag{61}$$

Observe that the time integration was extended over all time intervals in which σ is positive, and the maximum is taken over all pairs of initial states.

Due to its simplicity and intuitive physical interpretation, these measures are widely and commonly used in the study of non-markovianity in quantum systems.

6.4 MEASURES TO COMPARE QUANTUM CHANNELS

In order to compare evolutions, regarding the geometric measure in Section 6.3.1, we present now measures capable of comparing two quantum channels. Of course a good measure must have a useful operational interpretation, satisfy properties for theoretical reasoning and ideally be easy to compute. For example, if $\rho_1' = \Lambda_1(\rho)$ and $\rho_2' = \Lambda_2(\rho)$, the trace norm of $\rho_1' - \rho_2'$ determines how well ρ_1' and ρ_2' can be distinguished. In this section we review two measures which have an operational interpretation in terms of channel discrimination.

6.4.1 Diamond Norm

In order to introduce the diamond norm, also known as *completely bounded trace norm*, let us imagine the following situation: We have access to quantum channels that we know are either Λ_1 or Λ_2 with probabilities α and $1-\alpha$, respectively. The probability of success in a single shot for distinguishing Λ_1 or Λ_2 is given by

$$p = \frac{1}{2} + \frac{1}{2} \parallel \alpha\Lambda_1 - (1-\alpha)\Lambda_2 \parallel_1 . \tag{62}$$

The 1-norm of a channel Λ is given by

$$||\Lambda||_1 = \max\{||\Lambda(A)||_1 : A \in \mathcal{H}(A), ||A||_1 \leq 1\}. \tag{63}$$

Note that A is some operator whose 1-norm was defined in Section. 2.5.

If the channels are randomly chosen and we know nothing about the probability of being Λ_1 or Λ_2, we assume that $\alpha = 1/2$, and

$$p = \frac{1}{2} + \frac{1}{4} \parallel \Lambda_1 - \Lambda_2 \parallel_1 . \tag{64}$$

Observe that as mentioned before, $\parallel \Lambda_1 - \Lambda_2 \parallel_1$ is not a good definition to distinguish quantum channels. The main reason behind is that it is not possible to explore quantum entanglement to increase the distinguishability, an interesting work related to this was developed in (RIVAS et al., 2010). For a perfect discrimination, an ancillary Hilbert space $\mathcal{K}$ with dimension equal to that of the input, even when the output dimension is much smaller, is required. Consequently the input states are now ξ defined in $\mathcal{K} \otimes \mathcal{H}$. The output states to be discriminated are now $(\mathbb{1}_{\mathcal{K}} \otimes \Lambda_1)\xi$ and $(\mathbb{1}_{\mathcal{K}} \otimes \Lambda_2)\xi$. Consequently, the probability of success reads

$$p = \frac{1}{2} + \frac{1}{4} \parallel \Lambda_1 - \Lambda_2 \parallel_\diamond, \tag{65}$$

where the diamond norm $\parallel \Lambda \parallel_\diamond$ is given by

$$\parallel \Lambda \parallel_\diamond \equiv \max_{\xi} \parallel (\mathbb{1}_{\mathcal{K}} \otimes \Lambda_1)\xi \parallel_1 \tag{66}$$

Working on the above equation, we may define the *diamond norm distance* between the channels as

$$\parallel \Lambda_1 - \Lambda_2 \parallel_\diamond = \sup_{\xi} \parallel (\mathbb{1}_{\mathcal{K}} \otimes \Lambda_1)(\xi) - (\mathbb{1}_{\mathcal{K}} \otimes \Lambda_2)(\xi) \parallel_1, \tag{67}$$

where $\mathbb{1}_{\mathcal{K}}$ denotes the identity map. The supremum is always achieved, provided $dim(\mathcal{K}) \geq dim(\mathcal{H})$.

It is possible to proof that the diamond norm is bounded (WATROUS, 2012; KLIESCH et al., 2016), as can be seen below

$$\frac{1}{n} \parallel \Lambda_1 - \Lambda_2 \parallel_\diamond \leq \parallel J(\Lambda_1) - J(\Lambda_2) \parallel_1 \leq \parallel \Lambda_1 - \Lambda_2 \parallel_\diamond, \tag{68}$$

where n is the normalization factor. In other words, the dimension of $\mathcal{H}$ and $J(\Lambda)$ is the Choi-matrix associated to Λ, as presented in Chapter. 3. For the validity of the second inequality we are considering $\xi = 1/n \sum_{1 \leq i,j \leq n} |i\rangle\langle j| \otimes |i\rangle\langle j|$. Back to Eq. 65, it is easy to observe that depending on the choice of Λ_1 and Λ_2, the channels can be perfectly distinguishable ($\parallel \Lambda_1 - \Lambda_2 \parallel_\diamond = 2$).

The diamond norm is not easy to compute. There are limited analytical expressions that can be obtained, and only in special cases. Basically most algorithms developed to calculate it are based on semi definite programming, which is a special class of convex optimization, that use sophisticated algorithms to find the optimal value. Due to its complicate evaluation, we present an algorithm developed in (BENENTI; STRINI, 2010) to compute the diamond norm numerically using Monte Carlo.

6.4.1.1 F-algorithm

Called *F-algorithm*, for using the Fano representation (FANO, 1957), the algorithm consists in optimizing the trace norm over a large number of randomly chosen input states ξ. For one-qubit channels, it is sufficient to add a single ancillary qubit when computing the diamond norm (KLIESCH et al., 2016). A convexity argument shows that it is enough to take the maximum only over pure states (BENENTI; STRINI, 2010). Then, $\xi = |\psi\rangle\langle\psi|$, where $|\psi\rangle$ is a two-qubit state. As presented in Chapter 2, the state of a qubit can be written in terms of the coordinates of the Bloch vector $\vec{r}$. In the Fano-form, $\vec{r} = (x, y, z, 1)^T$. The transformation of the Bloch vector induced by a quantum channel Λ_i is directly determined by

$$\vec{r_i'} \equiv \mathcal{M}_i^{(1)}\vec{r},$$

where $\mathcal{M}_i^{(1)}$ is a 4×4 affine transformation matrix. In order to represent the quantum operations $\mathbb{1}_{\mathcal{K}} \otimes \Lambda_i$, we define

$$\mathcal{M}_i^{(2)} \equiv \mathbb{1}^{(1)} \otimes \mathcal{M}_i^{(1)}.$$

These 16×16 affine transformation matrix maps the 16×1 vectors $\mathbf{R}$ into $\boldsymbol{R_1'} = \mathcal{M}_1^{(2)}\boldsymbol{R}$ and $\boldsymbol{R_2'} = \mathcal{M}_2^{(2)}\boldsymbol{R}$. The vector $\boldsymbol{R}$ is a column vector of real coefficients $R_{\alpha\beta}$

$$R_{\alpha\beta} = Tr[(\sigma_\alpha \otimes \sigma_\beta)\xi],$$

with $\alpha, \beta = x, y, z, I$ labeling the well known Pauli matrices $\sigma_x, \sigma_y, \sigma_z$ and $\sigma_I = \mathbb{1}$. Finally, it is possible to represent any two-qubit state in the Fano form:

$$\xi = \frac{1}{4}\sum_{\alpha,\beta} R_{\alpha\beta}\sigma_\alpha \otimes \sigma_\beta. \tag{69}$$

The trace distance is then computed between the output states $\xi_1' = (\mathbb{1}_{\mathcal{K}} \otimes \Lambda_1)(\xi)$ and $\xi_2' = (\mathbb{1}_{\mathcal{K}} \otimes \Lambda_2)(\xi)$

$$\| \xi_1' - \xi_2' \|_1 = \sum_k |\lambda_k|, \tag{70}$$

where $\lambda_1, ...\lambda_k$ are the eigenvalues of $\xi_1' - \xi_2'$.

Computing the F-algorithm is quite straightforward and easily implemented in the most commonly used programming languages. Another alternative to compute the diamond norm is to obtain directly the Kraus representation from ξ_1' and ξ_2'. But, in most cases, it is not easy to obtain the Kraus operators.

Another advantage of the F-algorithm is that the matrix elements of $\mathcal{M}_i$ give us a clear physical interpretation of the transformations of the expectation values of the system's polarization measurements. This can be easily seen because the matrix elements

of $\mathcal{M}_i$ represent the transformation on the Bloch vector, that is directly related to the polarization of a qubit.

7 APPLICATION

"All you have to do is move people just a little bit for changes to happen. It doesn't have to be something huge."

Viola Davis

In this chapter we propose an approach to study non-Markovian evolutions. By exploring the idea of replacing non-physical inverse evolutions by the Petz recovery map, widely discussed in the Chapter 5. We show that it is even possible to attenuate non-Markovian undesired effects using this strategy.

7.1 APPLICATION

In order to investigate non-Markovian evolutions from the Petz recovery map perspective, we recall the divisibility property for quantum maps in Eq. 48. Without loss of generality, choosing $t_0 = 0$ we obtain

$$\Lambda_{t_2,0} = \Lambda_{t_2,t_1}\Lambda_{t_1,0}, \text{ for } t_2 \geq t_1 \geq 0. \tag{71}$$

The equation above describes the dynamics of a quantum state from 0 to t_2. The intermediate map Λ_{t_2,t_1} can be defined as

$$\Lambda_{t_2,t_1} = \Lambda_{t_2,0}\Lambda_{t_1,0}^{-1}. \tag{72}$$

Recalling section 6.1, if Λ_{t_2,t_1} is not CP, the dynamics will be non-Markovian. Observe that the intermediate map is written in terms of the inverse map $\Lambda_{t_1,0}^{-1}$, which in most cases is not a CP map. Many times the map $\Lambda_{t_1,0}$ is not invertible and consequently the intermediate map is not well defined. This is a way to think of it as a lack of information about the process. Based on what was developed in the previous chapter, we propose to replace the inverse map of $\Lambda_{t_1,0}$ by the Petz recovery map

$$\Lambda_{t_1,0}^{-1} \approx \Lambda_{Petz}.$$

We would like to define an approximate intermediate map given by

$$\Lambda_{t_2,t_1}^{approx} = \Lambda_{t_2,0}\Lambda_{Petz}. \tag{73}$$

Since the Petz is a completely positive map, it is possible to construct a new dynamics where the problem of the inverse not being CP was solved. Note that by doing this, we

guarantee now that the intermediate map is CP. Replacing in Eq. 48 the intermediate map by Eq. 73, we obtain the total dynamics given by

$$\Lambda_{t_2,0}^{approx} = \Lambda_{t_2,0}\Lambda_{Petz}\Lambda_{t_1,0}. \tag{74}$$

7.2 NON-MARKOVIAN DEPHASING

Recalling section 6.2, we construct a non-Markovian evolution for a qubit choosing $\gamma_1(t) = 1$ and $\gamma_2(t) = \sin(t)$. It is easy to see that $\Gamma_1 = t$ and $\Gamma_2 = 1 - \cos(t)$. The evolution is clearly non-Markovian since $\gamma_2(t) = \sin(t)$ is periodic and can assume negative values for some time intervals (CHRUŚCIŃSKI; WUDARSKI, 2013). Equation 30 can then be rewritten in terms of a new probability distribution defined as

$$p_1^{deph}(t) = \alpha(1 - e^{-2(1-\cos(t))}), \tag{75}$$

where $\alpha = e^4/(e^4 - 1)$. It is a periodic function of period 4π as can be seen in Fig. 10. In order to investigate a different behavior, we propose another dephasing model, defined by the following probability distribution

$$p_2^{deph}(t) = 1 - e^{-0.3\cos^2 t}. \tag{76}$$

This model has an interesting behavior, it is a damped oscillation which stabilizes in $p_2^{deph}(t) = 1$, for longer times. From this point on, we classify both dynamics above as Case 1 and Case 2, for $p_1^{deph}(t)$ and $p_2^{deph}(t)$.

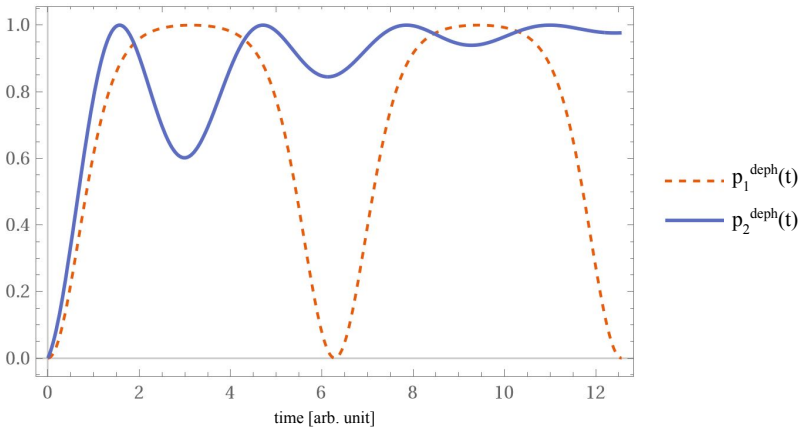

Figure 10 – Probability distributions characterizing a non-Markovian dephasing evolution.

Both evolutions above define the original non-Markovian dynamics $\Lambda_{t_2,0}$. For simplicity let us replace $t_2 = t_f$ and $t_1 = t$. In the following subsections we analyze our strategy for the two different situations: the evolution is free going from $t_0 = 0$ to the final time $t_f = 2t$, and when the evolution is fixed with $t_f = 2\pi$.

7.2.1 Final time free in 2t

This is the case of an evolution occurring in an unlimited time interval. We deal with only one parameter t. Equation 48 is rewritten as

$$\Lambda_{2t,0} = \Lambda_{2t,t}\Lambda_{t,0}. \tag{77}$$

Consequently, the same happens to $\Lambda^{approx}_{2t,0} = \Lambda^{approx}_{2t,t}\Lambda_{t,0}$. We begin by verifying the positiveness of the dynamics through Fig. 11. As discussed in Chapter 3, the eigenvalues of the Choi Matrix are positive if the map is CP.

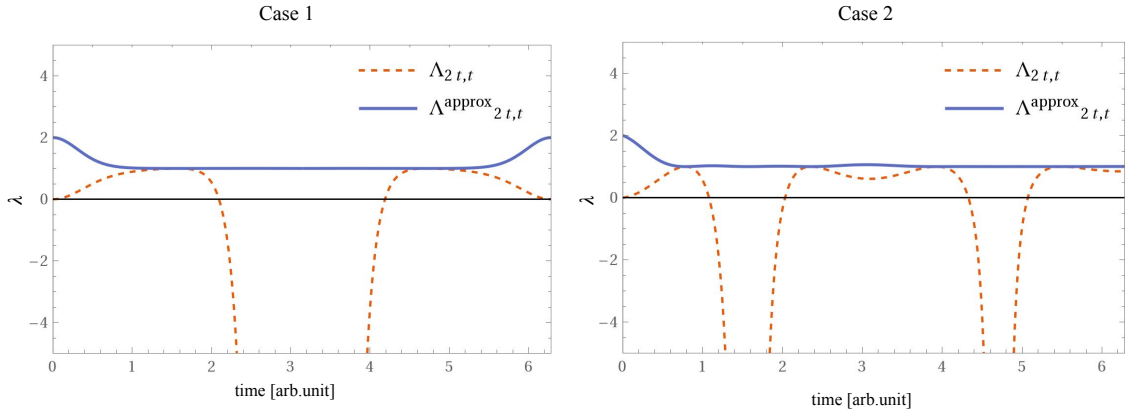

Figure 11 – Plot of the smallest eigenvalues λ of each one of the intermediate dephasing maps $\Lambda_{2t,t}$ and $\Lambda^{approx}_{2t,t}$.

We noticed that the smallest eigenvalue of $\Lambda^{approx}_{2t,t}$ is positive for all times no matter what probability distribution $p_i^{deph}(t)$ we choose. As expected, since by construction $\Lambda^{approx}_{2t,t}$ is CP. On the other hand, for the $\Lambda_{2t,t}$ map, there is a negative eigenvalue for some time intervals, consequently, this evolution cannot be classified as CP. Observe that the minimal value of the most negative λ, occurs in the limit of non-bijectivity, we can confirm this by looking to Fig. 10. Observe that both eigenvalues in Fig. 11, are most different as possible at this regime of non-bijectivity. It is also interesting to observe that there is some time intervals where λ of $\Lambda_{2t,t}$ is positive. For the Case 1, when $t \in [1.4, 1.8]$ and $t \in [4.6, 5]$ the minimum eigenvalue of $\Lambda^{approx}_{2t,t}$ is equal to the minimum eigenvalue of $\Lambda_{2t,t}$. In other words, since the eigenvalues are directly related to the Kraus operators, we can say that the maps are equal at these points. It is easy to prove that all the eigenvalues, even the larger ones coincide at these points, a property of the Kraus operators, discussed in Chapter 3.

For Case 2, the behavior is quite similar. We noticed that due to the form of $p_2^{deph}(t)$, the value of λ oscillates more frequently. In a more detailed analysis, the valleys on the negative semi-axis are narrowing over time. Also, the separation between the ridges on the positive semi-axis is less pronounced. The negative eigenvalue becomes more positive

over time. Contrary to what happens in the first case, this can be understood since $p_2^{deph}(t)$ is stabilizing for $t >> 2\pi$. Initially we can be led to believe that the new proposed dynamics is Markovian. To find out if this is indeed true, we use the already presented trace distance in Section 2.5 and again discussed in Section 6.3. The idea behind is that for Markovian processes the trace distance is a monotonically decreasing function in time. In other words, under a Markovian evolution any two initial states can never become more distinguishable over time.

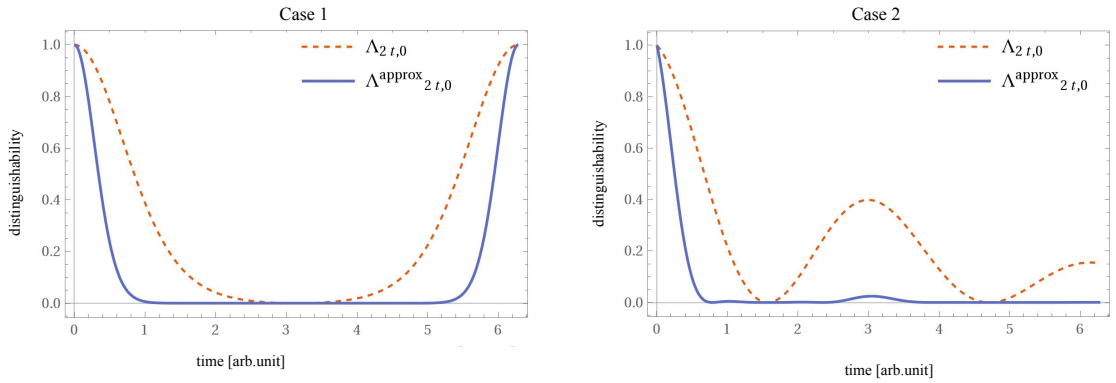

Figure 12 – Distinguishability between two states $D_{tr}(\rho_1, \rho_2)$ over time for dephasing. With $\rho_1 = |+\rangle\langle+|$ and $\rho_2 = |-\rangle\langle-|$ for both cases.

We took two initial orthogonal states $\rho_1 = |+\rangle\langle+|$ and $\rho_2 = |-\rangle\langle-|$. Looking at Fig. 12, they are completely distinguishable at the beginning of the evolution, as expected. However, for the proposed dynamics $\Lambda_{2t,0}^{approx}$ there is still an increase of the distinguishability between the two states, therefore being still NM. This can be explained if we look back to Eq. 74. The total dynamics is CP but is not CP-divisible, since there is still a dependence from the original NCP dynamics $\Lambda_{t_2,0}$ treated here as $\Lambda_{2t,0}$.

It could be also noticed that for the Case 1, the effects of non-Markovianity are stronger than in the Case 2, whose revival occurs but is smaller. We can state, especially for the second case, that apparently a large part of the non-Markovian effects were suppressed using this approach. There is a simple reason for this to happen. If we go back to Fig. 10, and analyze it from a physical perpective, we notice that $p_1^{deph}(t)$ induces a drastic change of the state undergoing this evolution. Observe that when $p_1^{deph}(t) = 1$ the map is completely dephasing, the state was driven to one possible state of the image set, stays there for a considerable time and then is drived back to the initial point. On the contrary, the second probability induces a smooth change, it is happening by parts until finally stabilizes in the completely dephased state for longer times. We can think of it as a thermalization process, when a stationary state is reached for $t \to \infty$. This kind of oscillatory behavior is found in damped oscillators.

Another issue to be addressed here is the similarity between the original NM dynamics and the new proposed dynamics. To do so, we use the formalism presented in Section 6.4. We observed that $||\Lambda_{2t,0}^{approx} - \Lambda_{2t,0}||_\diamond = ||J(\Lambda_{2t,0}^{approx}) - J(\Lambda_{2t,0})||_1$. Then, for simplicity, to avoid the maximization required to compute the diamond norm, we opted to investigate the trace distance between the Choi matrices shown in Fig. 13 for both cases 1 and 2. For this calculation we still used the Fano algorithm; however, we applied the map only to one of the Bell states.

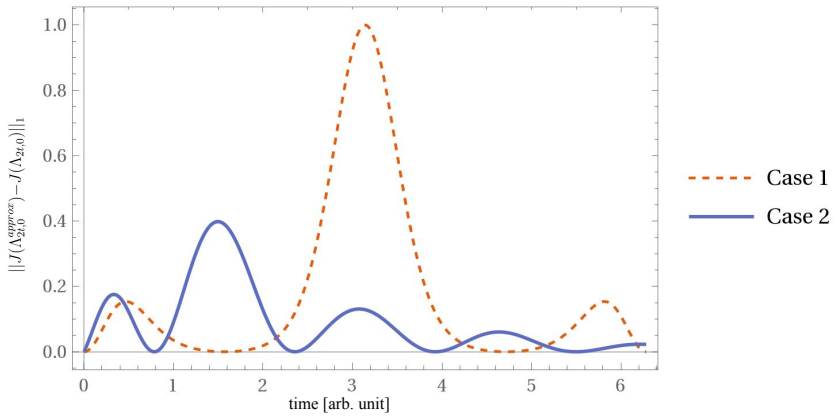

Figure 13 – Distance between the Choi matrices over time for both cases for a dephasing channel.

The above Figs. 11 and 13 can be seen as complementary ones. For the Case 1, we observe that the peaks in 13 occur in the same time interval when the eigenvalues in Fig. 11 are so discrepant. The same line of thinking applies when the distance between the maps is zero, which occurs when the $\lambda's$ are equal.

For the second case, an increase in distance is also observed when the eigenvalues are different, reaching peaks when the discrepancy between them is as large as possible. Similarly, the distance is null in the time intervals when the eigenvalues of $\Lambda_{2t,t}$ and $\Lambda_{2t,t}^{approx}$ coincide. This behavior is explained by the fact that when the eigenvalue of the Choi matrix of a map becomes positive, the map is completely positive. It is expected that the distance between a CP map and another CP map to be smaller than the distance between a CP and a NCP map. As seen in the Fig. 12, the proposed CP dynamics indeed reduce non-Markovian effects. For example, a simple way to verify this is the difference between the values of the distance between the Choi matrices for the different cases. For Case 1, the value is much larger than for Case 2. This means that our proposed dynamics works better when the evolution is described by $p_2^{deph}(t)$. We noticed that as time goes by, $\Lambda_{2t,0}$ and $\Lambda_{2t,0}^{approx}$ become hard to distinguish. Contrary to the Case 1, when the distance is "periodic". The same behavior will be observed if we plot from $t = 2\pi$ to $t = 4\pi$ or from $t = 4\pi$ to $t = 6\pi$, and so on. Of course this happens due the fact that the related time

dependent probability distribution $p_1^{deph}(t)$ is also periodic.

Finally we arrived at the main point of this analysis, the success of the proposed strategy is strongly correlated to the probability distribution which defines the evolution. We can think that the probabilities $p_{i's}(t)$ are related to the correlations between the system and the environment or bath, for example. It determines how the evolution will develop, if the steady state will be reached quickly, slowly, and how the information flow between system and environment will occur.

This is an interesting result because it opens the possibility to study different non-Markovian dynamics. It is worth to mention that most physical phenomena are in fact non-Markovian, but not always easily to be understood. With this strategy, it would be possible to investigate the similarity between a non completely positive and consequently non-physical map, inside a NM evolution and a CP one.

7.2.2 Final time fixed

Now we look for a fixed evolution, when the final time is previously set. We provide here two examples, the first one with $t_f = 2\pi$ and the second one with $t_f = 4\pi$. The strategy is the same as the one used before, we have two time dependent probability distributions $p_1^{deph}(t)$ and $p_2^{deph}(t)$ defined in Eqs. 75 and 76, corresponding to the cases 1 and 2, respectively.

Fixed final time $t_f = 2\pi$ The corresponding evolution can be written as

$$\Lambda_{2\pi,0} = \Lambda_{2\pi,t}\Lambda_{t,0}. \tag{78}$$

The approximate dynamics is also changed to

$$\Lambda_{2\pi,0}^{approx} = \Lambda_{2\pi,t}^{approx}\Lambda_{t,0}, \tag{79}$$

where $\Lambda_{2\pi,t}^{approx} = \Lambda_{2\pi,0}\Lambda_{Petz}$. In order to verify the completely positiveness of the dynamics, we look for the eigenvalues λ of the Choi matrix of the intermediate map. Looking for Fig. 14, we observe a similar behavior to what was presented before for $t_f = 2t$. Our proposed dynamics has positive eigenvalues, being a CP map, as expected for both Cases 1 and 2. The main difference now is that the intermediate map from the original dynamics $\Lambda_{2\pi,t}$ is "less positive"compared to the previous analysis. For Case 1 there is no regime where λ is positive contrary to Fig. 11. For Case 2 we observe that this regime of positivity is getting smaller over time, until it vanishes as can be seen for $t > 3\pi/2$. In order to give a better explanation, let us analyze the dynamics for $t_f = 4\pi$.

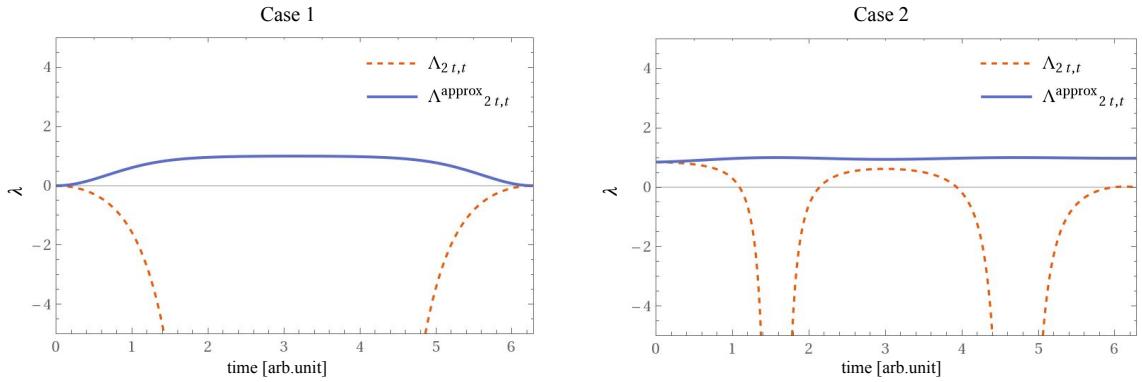

Figure 14 – Plot of the smallest eigenvalues λ of each one of the intermediate dephasing maps $\Lambda_{2\pi,t}$ and $\Lambda^{approx}_{2\pi,t}$.

Fixed final time $t_f = 4\pi$ Quite similar to the previously mentioned example, we want to compare the evolutions $\Lambda_{4\pi,0}$ and $\Lambda^{approx}_{4\pi,0}$. This example illustrates well the main difference between the behaviors of the probability distributions.

Complementary to Fig. 14, Fig. 15 shows the behavior of the eigenvalues over time when we extend the final time. As expected, for the Case 1 we have a periodic function for λ, quite similar to $p_1^{deph}(t)$ that is also a periodic function. For Case 2, as already mentioned, there is a decrease in the regime in which the eigenvalues are positive. Much like what happens when $t_f = 2t$ in Fig. 11, but in a less subtle way. We also observe that for a fixed dynamics, there is a boundary as can be observed comparing the Figs. 14 and 15, especially for the Case 2.

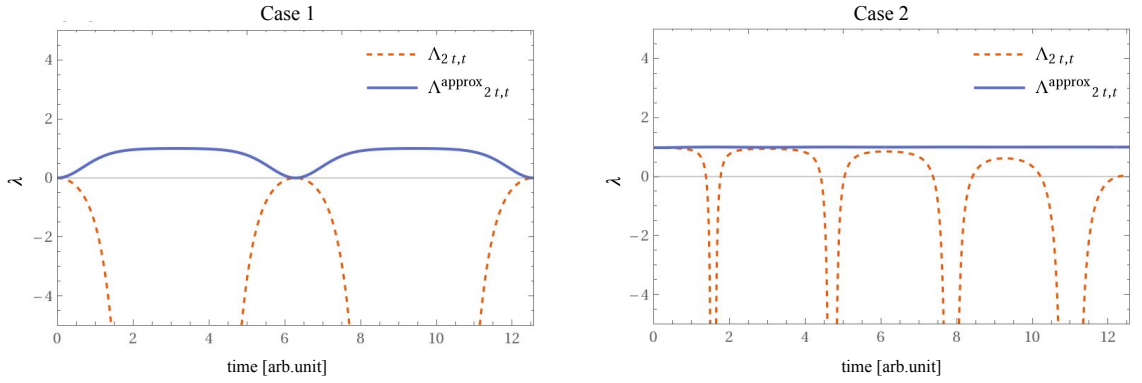

Figure 15 – Plot of the smallest eigenvalues λ of the Choi matrix of the intermediary maps $\Lambda_{4\pi,t}$ and $\Lambda^{approx}_{4\pi,t}$.

To summarize, we look for Fig. 16 that shows the distances between the Choi matrices for $t_f = 2\pi$ and $t_f = 4\pi$. The first thing to be observed is that for Case 1, the distance is now larger than the one showed in Fig. 13, meaning that the dynamics is more different when we set the time to a fixed value.

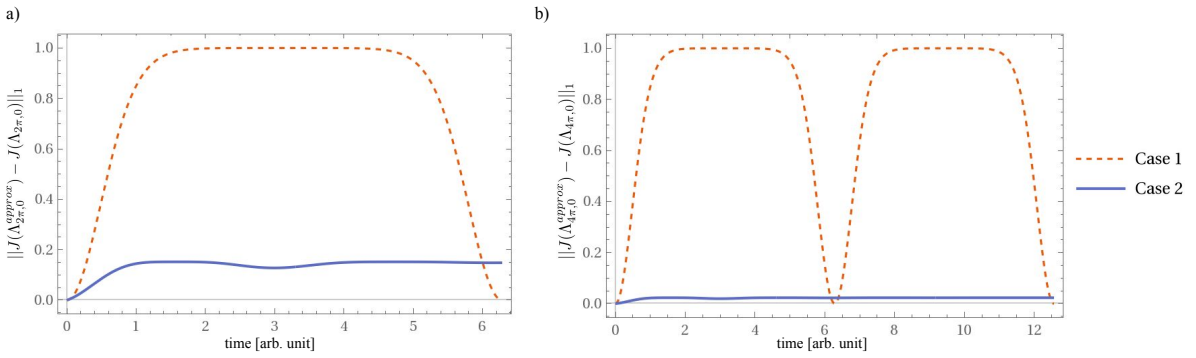

Figure 16 – Choi distances for both cases with final time fixed. In a) $t_f = 2\pi$ and b) $t_f = 4\pi$.

For Case 2 the distance gets smaller when we fix the final time t_f, and even smaller for $t >> 2\pi$. This can be easily understood if we look at the probabilities in Fig. 10. Note that $p_2^{deph}(t)$ slightly oscillates and then starts to stabilize at its maximum value equal to 1. What happens to the map in this time frame? Basically it is a maximum dephasing that comes back and forth due to the non-Markovianity effects, represented here by these oscillations. When we fix the time, it is as if we limited the dynamics to stabilize more quickly, decreasing these oscillations. The point is that now, as already mentioned, the eigenvalues of the original dynamics are less positive, which makes it difficult for a CP map to perfectly simulate a NCP one. For this reason, although the distance has now decreased and does not fluctuate, it will never reaches zero, unlike what we get with a non-fixed time. For even bigger times, we have reached the regime where the dynamics $\Lambda_{4\pi,t}$ is even more stable as can be verified in Fig. 10. For this reason, the distance is even smaller.

We can think in dynamics with a fixed time to occur when the system is not evolving for an unlimited time interval. This can be quite interesting if we are interested in building a dynamics which happens in a short period of time. An atom decays with a short half-life. Or even if we set the final time because what comes next does not interest us anymore.

7.3 NON-MARKOVIAN DEPOLARIZING

In this section we will repeat the same analysis for the depolarizing channel. Following the lead of (CHRUŚCIŃSKI; WUDARSKI, 2013), since the depolarizing is also a random unitary evolution as presented in Eq. 52, we define the first probability distribution as

$$p_1^{depol}(t) = \beta(1 - e^{-2(1-\cos(t))}), \tag{80}$$

where $\beta = 3e^4/4(e^4 - 1)$. It has the same periodic behavior as $p_1^{deph}(t)$.

We also look to another depolarizing model. After resizing $p_2^{deph}(t)$ to satisfy Eq. 31, we obtain

$$p_2^{depol}(t) = \frac{3}{4}(1 - e^{-0.3\cos^2 t}). \tag{81}$$

From this point on, we maintain the classification used in the last section. We use Case 1 and Case 2 for $p_1^{depol}(t)$ and $p_2^{depol}(t)$, respectively.

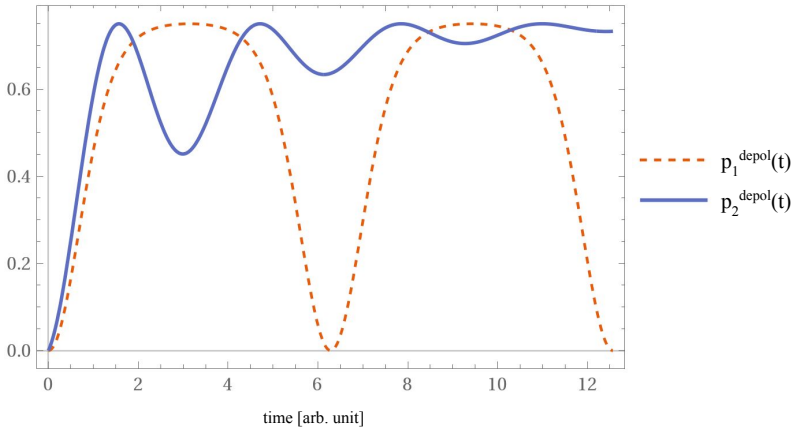

Figure 17 – Probability distributions characterizing a non-Markovian depolarizing evolution.

7.3.1 Final time free in 2t

From now on, what comes next is quite straightforward. We will analyze again $t_f = 2t$, replacing $\Lambda_{t_2,0} = \Lambda_{2t,0}$ and $\Lambda_{t_2,t_1} = \Lambda_{2t,t}$, with $\Lambda = \Lambda_{depol}$, defined in Eq. 31. We begin by analyzing the complete positiveness of our proposed dynamics $\Lambda_{2t,0}^{approx}$ compared to the original NM ones.

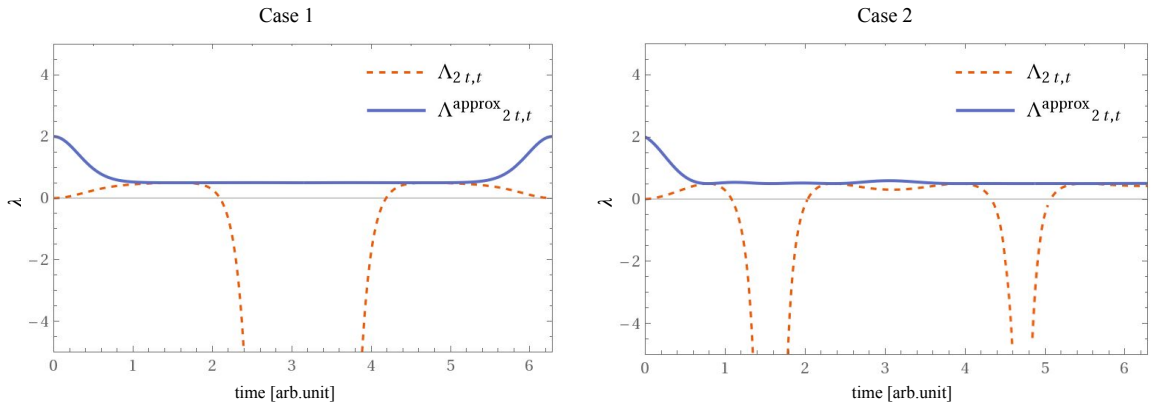

Figure 18 – Plot of the smallest eigenvalues λ of the Choi matrix of each one of the intermediate depolarizing maps $\Lambda_{2t,t}$ and $\Lambda_{2t,t}^{approx}$.

At first, we notice the similarity between Fig. 11 and Fig. 18. Both smallest eigenvalues of $\Lambda_{2t,t}^{approx}$ are positive for all times. We keep obtaining a CP dynamics as expected. What is interesting is that the eigenvalues are smaller compared to the dephasing

evolution. Despite having the same time intervals when $\Lambda_{2t,t}$ is positive, the maximum positive value obtained is now smaller than the one in Fig. 11.

For the Case 2, specifically, we observe again in Fig. 18 the narrowing of the valleys on the negative semi-axis over time and the decrease in the separation between the ridges on the positive semi-axis. For $t > 3\pi/2$, the ridges begin to disappear into a plateau.

From the previous section, we know that we are not building a Markovian dynamics. Besides the map $\Lambda^{approx}_{2t,0}$ is CP, it is not CP-divisible. Even so, it is interesting to compare how the distinguishability varies over time for different evolutions. We used the same initial states ρ_1 and ρ_2 as in the previous section.

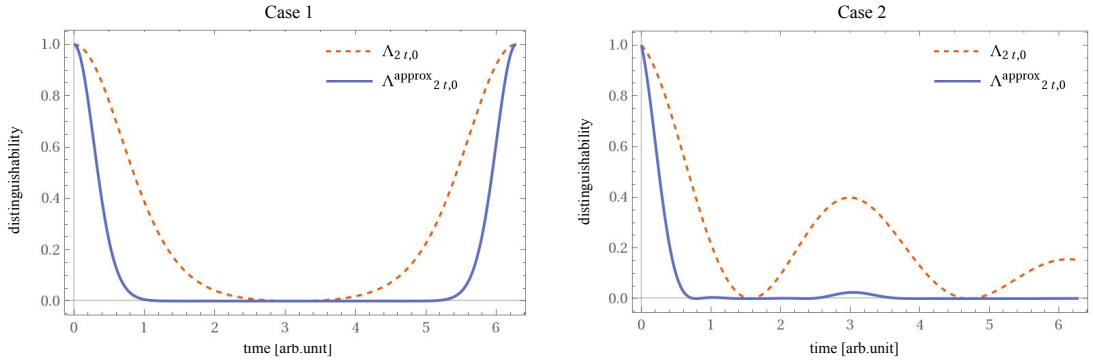

Figure 19 – Distinguishability between two states $D_{tr}(\rho_1, \rho_2)$ over time for depolarizing. With $\rho_1 = |+\rangle\langle+|$ and $\rho_2 = |-\rangle\langle-|$ for both cases .

The Fig. 19 shows the distinguishability between ρ_1 and ρ_2 over time for the original and approximated maps. We noticed that it is quite similar to Fig. 12. The reason behind this is that we are using the same probabilities, they just were resized to satisfy the dynamical maps defined in Chapter 3. Again the proposed CP dynamics indeed reduce the non-Markovian character of the evolution.

However, this is not all. If we look to Fig. 18, when $t = \pi$ the eigenvalues are completely different. This is the regime of non-bijectivity. Observe that at this point, the states are not distinguishable, since the map drove ρ_1 and ρ_2 to the maximally mixed state. However, the distinguishability starts to grow around $t = 5.2$. This confirms that our proposed dynamics is not Markovian, because as already mentioned, it is still not CP-divisible. There is no new information from Case 2. The distinguishability decreases for both evolutions. Then around $t = \pi/2$ it starts growing for the original dynamics, but surprisingly, the CP one only starts growing around $t = \pi$ until it reaches the value of 0.1 approximately. After this, it decreases to zero and remains there.

Again, we are dealing with two evolutions defined by different probabilities and

consequently with two different performances of the Petz recovery map. However, it is worth mentioning that non-Markovianity effects were suppressed by the proposed dynamics.

Regarding the distance between the dynamics shown in Fig. 20, it is possible to identify right away that the distance $||J(\Lambda_{2t,0}^{approx}) - J(\Lambda_{2t,0})||_1$ is larger than for the dephasing channel. For Case 1, we now have the maximum value of the distance equal to 1.5. This agrees with the results presented in Chapter 5, since the Petz recovery map is in fact able to better recover states from the dephasing evolution, something justified here by the degree of non-invertibility of the channels. For Case 2, the values are also larger than for the previous quantum channel, what confirms that the maps are now a little bit more different. Basically the Petz is a little bit less effective for this channel. Apart from the numerical values, the shapes of the curves for both cases are equal compared to Fig. 13. Of course, something that is expected since we maintained the behavior of the probability distribution functions.

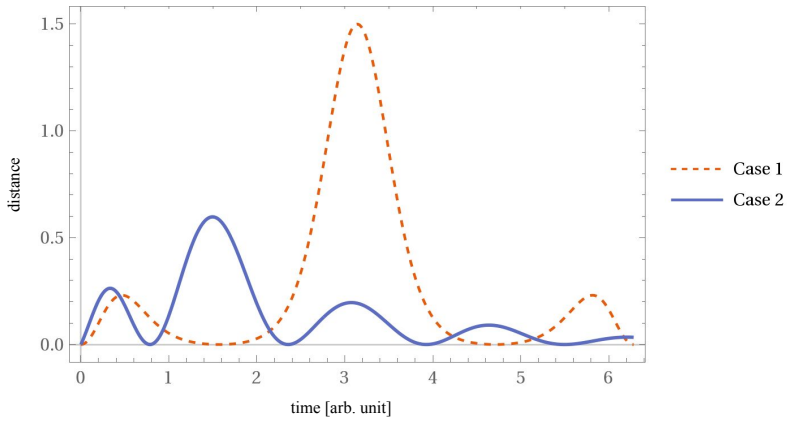

Figure 20 – Distance between the Choi matrices over time for both cases for a depolarizing channel.

Regarding Fig. 18, we noticed that the peaks in Fig. 20 occur in the same time interval when the eigenvalues are completely different. Also, the distance is zero in the time intervals where the eigenvalues for $\Lambda_{2t,t}$ and $\Lambda_{2t,t}^{approx}$ coincide.

Due to its similarity with the previous channel, we are not concerned in repeating the same analysis for $t_f = 2\pi$.

7.4 NON-MARKOVIAN AMPLITUDE DAMPING

The analysis for the amplitude damping is a little bit different. First of all, it is not a random unitary evolution like the other two. This means that the approach used in the previous sections to construct a non-Markovian evolution cannot be used again

for this channel. Second, the amplitude damping is not a unital map, for this reason the calculations are a little bit more complicated.

Based on the book (NIELSEN; CHUANG, 2000), we assumed the following probability distribution

$$p_1^{a.d}(t) = \sin^2(t/2). \tag{82}$$

It is also a periodic function, quite similar to p_1^{deph} and p_1^{depol}, but the peak when $p_1^{a.d}$ reaches its maximal value is more accentuated and less like a plateau.

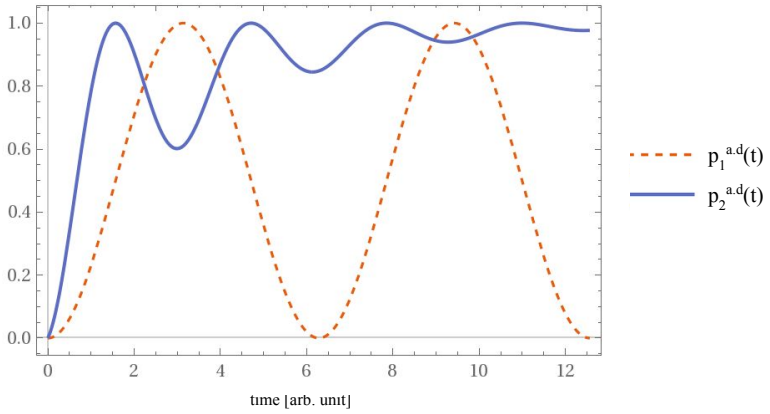

Figure 21 – Probability distributions characterizing a non-Markovian amplitude damping evolution.

The other evolution that we analyzed was described by the same probability as p_2^{deph} since it is not necessary to resize it. For this section we define the $p_2^{a.d} \equiv p_2^{deph}$. Both evolutions are shown in Fig. 21. From now on, we repeated the previous analysis, taking into account that Case 1 and Case 2 refers now to $p_1^{a.d}$ and $p_2^{a.d}$, respectively.

7.4.1 Final time free in 2t

Our evolution is again written as $\Lambda_{2t,0}$, where the evolution is now the amplitude damping channel, $\Lambda = \Lambda_{a.d}$, defined in Eq. 34. The complete positivity of the intermediate maps can be checked in Fig. 22.

What is interesting for this channel is that the smallest eigenvalue of the proposed CP dynamics $\Lambda_{2t,t}^{approx}$, the green curve in Fig. 22, is smaller than the positive eigenvalues of $\Lambda_{2t,t}$. A curious fact about this is that contrary to the other evolutions, there is no time intervals for $t \in (0, 2\pi]$ when all the eigenvalues coincide. The blue line corresponds to another eigenvalue of $\Lambda_{2t,t}^{approx}$, which coincides at some points with the negative eigenvalue of $\Lambda_{2t,t}$. This can be useful for our analysis.

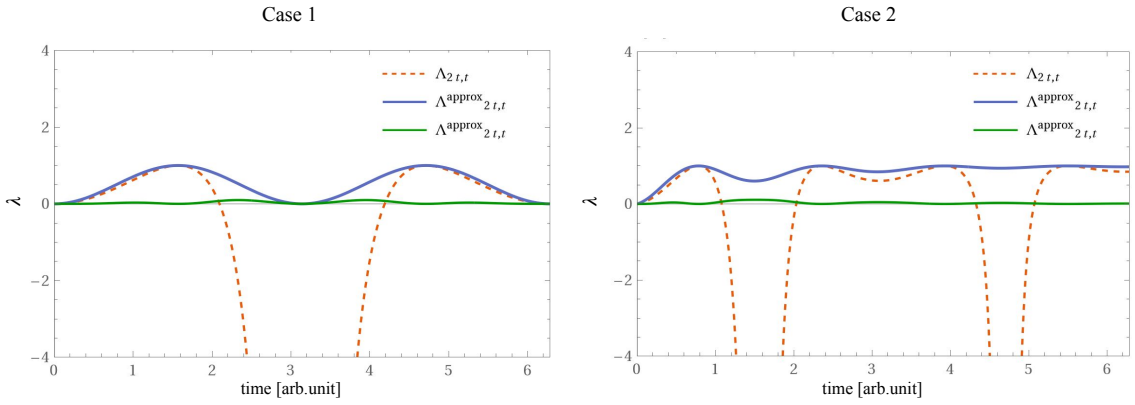

Figure 22 – Plot of the eigenvalues λ of the Choi matrix of the intermediary amplitude damping maps $\Lambda_{2t,t}$ and $\Lambda^{approx}_{2t,t}$. We plotted two eigenvalues of $J(\Lambda^{approx}_{2t,t})$.

For Case 1, we observe the negative eigenvalue with minimal point when $t = \pi$. This point corresponds to the limit of non-bijectivity, when $p_1^{a.d} = 1$, as can be seen in Fig. 21. There are also time intervals, for $t \in [0, 2.1]$ and again for $t \in [4.2, 6]$ where $\Lambda_{2t,t}$ is positive. When we look for Case 2, we confirm one more time what was mentioned before about the narrowing of the valleys on the negative semi-axis. This is explained due to the behavior of $p_2^{deph}(t)$ which is stabilizing for $t > 2\pi$. Until now, there is no brand new information about the dynamics.

In Fig. 23 we observe how the distinguishability varies over time for both cases. For Case 1, there is a decrease until $t = \pi$, and then non-Markovian effects begin to show up. It is worth to mention here the reason for this behavior. When $t = \pi$ we are at the limit of non-bijecivity (max amplitude damping), when all states were driven to the ground state $|0\rangle\langle 0|$. For $t > \pi$ the system is somehow recovering information and the states are distinguishable again. However, despite the growing of the curve for $\Lambda^{approx}_{2t,0}$, it grows less than for the original dynamics. For $t = 2\pi$, the system recovers all initial information, and the states were driven to the initial points. Just to remind, the Petz is not giving us this information, but the dynamics itself is taking charge of this. A remarkable characteristic of non-Markovian evolutions.

In the second case, the only difference is the presence of more oscillations. The distinguishability also reaches its minimum value in the regime of non-bijecivity, which happens approximately for $t = \pi/2$, $t = 3\pi/2$, $t = 5\pi/2$ and so on. Once again, we can state that, althought the new CP dynamics is still non-Markovian, it considerably reduces the effects of non-Markovianity present in the original non-Markovian one.

When we analyze the distance between the Choi matrices of the two maps, we certainly notice a peculiar behavior. Let us analyze it by parts. Looking for the dashed

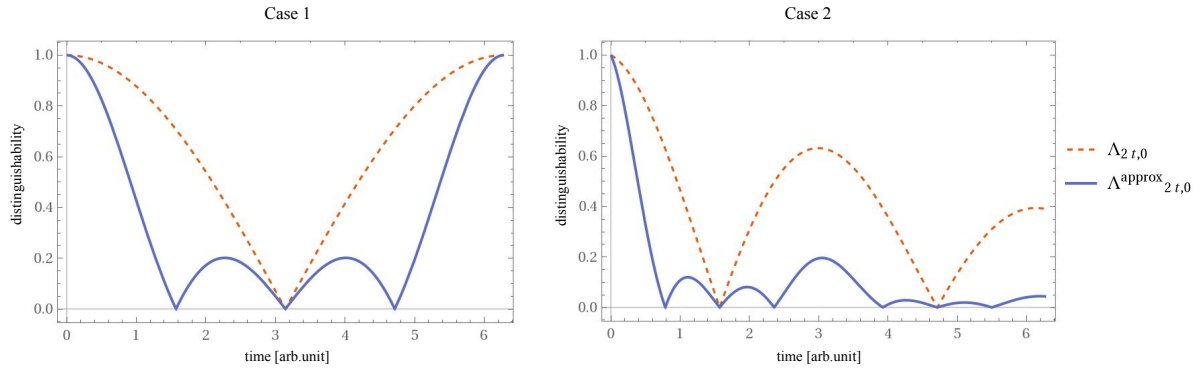

Figure 23 – Distinguishability between two states $D_{tr}(\rho_1, \rho_2)$ over time for amplitude damping. With $\rho_1 = |+\rangle\langle+|$ and $\rho_2 = |-\rangle\langle-|$ for both cases .

curve in Fig. 24, we see that the maximum value is around 1.75, larger than the values for the dephasing and depolarizing channel. Of course, we have chosen different probabilities, since now we are not dealing with Pauli channels. However p_1^{deph}, p_1^{depol} and $p_1^{a.d}$ have the same oscillatory behavior, with the same amplitudes. Another technicality is the fact that in Fig. 24, the *full width at half maximum (FWHM)*, is larger than in Figs. 13 and 20. Contrary to what happens with the probability, since the full width at half maximum is larger for p_1^{deph}, p_1^{depol}. We may ask ourselves now, what does this mean?

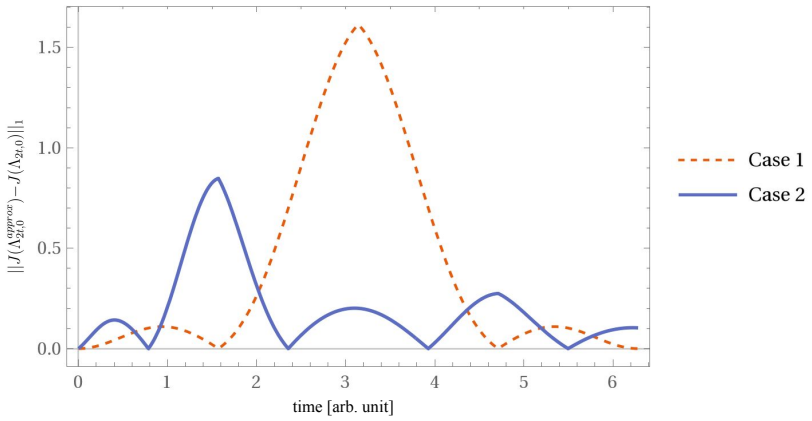

Figure 24 – Distance between the Choi matrices over time for both cases for an amplitude damping channel.

Well, if we compare the $p_1's$ in Figs. 10 and 21, the depolarizing follows the same line of thought, having a large FWHM means a slow growth towards the maximum. Basically the amplitude damping goes faster into the regime of non-bijectivity than the other two evolutions. That is why the distance is larger between the dynamics for more time intervals, simply because this reduces the possibility of the Petz in recovering the state and acting like an inverse. When we move to the regime of non-bijectivity we are

loosing information about the process, as was already discussed before.

For Case 2, the peaks are reached for $t = \pi/2$ and $t = 3\pi/2$, exactly when $p_1^{a.d} = 1$. The larger peak has an amplitude of approximately 0.8. The distance reaches zero when the eigenvalues coincide in Fig. 22. Compared to the other two channels, the amplitude damping has the worst performance. There is a peculiarity regarding this evolution. The peaks of the curves are not quite "smooth". They occur at the limit of non-bijectivity, that is when the Petz does not properly work at this point. It is a singularity, as mentioned in Chapter 5.

7.5 SUMMARY

With this strategy we conclude our approach to compute an inverse evolution through the Petz recovery map. We investigated that the invertibility degree proposed in Chapter 5 was in fact relevant to deal with non-Markovian evolutions.

All this analysis confirms the fact that the time dependent probability distribution $p(t)$ completely determines the positivity of the dynamics. Consequently it is a determining factor for the success of this strategy that we proposed. This can be understood in a simple way if we think in a system S interacting with an environment E. Depending on the correlations between S and E, the information flux between those two can be decisive for the emergence of irreversibility in the process.

Regarding non-Markovian dynamics there is still a plethora of open problems. One example that I consider especially interesting is related to *thermodynamics*. Quantum master equations as shown in Eq. 51 are not well indicated to describe thermodynamic properties of quantum systems, since we have no longer information about the global state $S + E$, and a lot of approximations are made. An alternative is to use *collisional models*, that allows full control over the interaction between the system S and tiny fractions of the environment, called ancillas A. What is interesting is that these models are fully described by a map Λ_{col} controlled by the experimentalist. From this model it is possible to derive the second law of thermodynamics for an open system (LANDI; PATERNOSTRO, 2020). If we now allow for the ancilla to interact with each other in a well defined manner we introduce non-Markovianity in the collisonal models (GARCÍA-PÉREZ et al., 2020). At this point our strategy can be useful and bring irreversibility into a new perspective.

8 CONCLUSION AND PERSPECTIVES

"Não se preocupe em entender. Viver ultrapassa todo entendimento. Renda-se como eu me rendi. Mergulhe no que você não conhece como eu mergulhei."

Clarice Lispector

In this work we investigated the concept of irreversibility for open quantum systems. We addressed the issue by reviewing the characterization of a qubit undergoing a physical evolution described by a quantum channel. Due to their numerous applications in quantum communication and computation, we chose to work with typical decoherence channels, such as dephasing, depolarizing and amplitude damping. We proposed to explore the Petz recovery maps to build an inverse quantum channel at the regime where an inverse map is not well defined. Our results demonstrated how the Petz can be useful to compute a completely positive inverse evolution. We showed that this is strongly related to the size of the image set at the non-bijectivity limit. Based on these results we defined an hierarchy between the dephasing, depolarizing and amplitude damping channels characterized by the non-invertibility degree of these decoherence processes. It is quite interesting if we think of it as an amount of information that we own about the system. This brings the possibility of application of this work to the field of quantum information theory and quantum computing, since we are able to construct a recovery map that gives us back information that was previously lost.

We also showed that, in certain situations, for a qubit undergoing a dephasing or depolarizing evolution, the same value of fidelity is achieved by simply doing nothing to the input state (identity map). However, as can be seen in (ŻYCZKOWSKI; SOMMERS, 2005), the fidelity between arbitrary states decays with the increase of the dimension N. Since $F(\rho, \sigma) \propto 1/N$. This is just a comment, the analysis itself was not done in this work, but the framework presented in this dissertation have risen new questions which could be the potential focus of subsequent work. The Petz recovery map could be more efficient in larger dimensions. One more time, it must be taken into account that, in this work, we analyzed the evolutions acting in the subspace of all one-qubit states. However, we may find ourselves restricted to certain constraints and bounds which change our domain where the map is acting. This is what I consider the central point of this study, in these specific

cases, for example, the Petz performance could be improved, and our analysis provide the necessary tools to find the best reference state and consequently the best recovery map.

Later we presented a general framework of Markovianity in open quantum systems, followed by measures to quantify the degree of non-Markovianity in an open system. The geometrical measure that compares two evolutions and calculates the distance between them; the RHP measure that identifies non-Markovian effects due to the violation of the divisibility property of the dynamical maps family; the BLP measure that quantifies the distinguishability between quantum states. In Chapter 7, we introduced a new strategy that can be quite useful to establish possible relations between non-Markovianity and other characteristics of an open quantum system, such as invertibility. We explored the results from Chapter 5 to build a physical evolution capable to simulate a non-completely positive one. Although a substantial reduction of non-Markovian effects has been achieved, it was not possible to build a Markovian evolution since the new proposed dynamics is CP but not CP-divisible. An interesting result obtained was the strong dependence of the success of this strategy with the initial correlations between the system and the environment, described by the time dependent probability distribution.

Another alternative would be to search the CP-divisible map closest to the original non-Markovian dynamics, as mentioned in Section 6.3. We may now ask ourselves how far is the Petz from this map? This is an open question. As discussed in Section 6.3, the geometrical measure could find the next Markovian dynamics. However a tricky optimization would be necessary.

REFERENCES

AL., M. J. et. Entropy, information and quantum measurements. **Annales Henri Poincare**, v. 19, p. 2955, 2018.

BELL, J. S. On the einstein podolsky rosen paradox. **Physics Physique Fizika**, American Physical Society, v. 1, p. 195–200, 1964.

BENENTI, G.; STRINI, G. Computing the distance between quantum channels: usefulness of the fano representation. **Journal of Physics B: Atomic, Molecular and Optical Physics**, IOP Publishing, v. 43, p. 215508, 2010.

BENGTSSON, I.; ZYCZKOWSKI, K.; MILBURN, G. **Geometry of quantum states: an introduction to quantum entanglement by Ingemar Bengtsson and Karol Zyczkowski**. [S.l.: s.n.], 2008. v. 8.

BERNARDES, N. K.; CARVALHO, A. R. R.; MONKEN, C. H.; SANTOS, M. F. Coarse graining a non-markovian collisional model. **Physical Review A**, American Physical Society (APS), 2017.

BORN, M. Zur Quantenmechanik der Stoßvorgänge. **Zeitschrift fur Physik**, v. 37, p. 863–867, 1926.

BREUER, H.; BREUER, P.; PETRUCCIONE, F.; PETRUCCIONE, S. **The Theory of Open Quantum Systems**. [S.l.]: Oxford University Press, 2002.

BREUER, H.-P.; LAINE, E.-M.; PIILO, J. Measure for the degree of non-markovian behavior of quantum processes in open systems. **Phys. Rev. Lett.**, American Physical Society, v. 103, p. 210401, 2009.

CHOI, M.-D. Completely positive linear maps on complex matrices. **Linear Algebra and its Applications**, v. 10, p. 285 – 290, 1975.

CHRUŚCIŃSKI, D.; RIVAS, A.; STORMER, E. Divisibility and information flow notions of quantum markovianity for noninvertible dynamical maps. **Phys. Rev. Lett.**, American Physical Society, v. 121, p. 080407, 2018.

CHRUŚCIŃSKI, D.; WUDARSKI, F. A. Non-markovian random unitary qubit dynamics. **Physics Letters A**, v. 377, p. 1425 – 1429, 2013.

DÜR, W.; VIDAL, G.; CIRAC, J. I. Three qubits can be entangled in two inequivalent ways. **Phys. Rev. A**, American Physical Society, v. 62, 2000.

EINSTEIN, A.; PODOLSKY, B.; ROSEN, N. Can quantum-mechanical description of physical reality be considered complete? **Phys. Rev.**, American Physical Society, v. 47, p. 777–780, 1935.

FANO, U. Description of states in quantum mechanics by density matrix and operator techniques. **Rev. Mod. Phys.**, American Physical Society, v. 29, p. 74–93, 1957.

GARCÍA-PÉREZ, G.; ROSSI, M. A. C.; MANISCALCO, S. Ibm q experience as a versatile experimental testbed for simulating open quantum systems. **npj Quantum Information**, v. 6, p. 1, 2020.

GORINI, V.; KOSSAKOWSKI, A.; SUDARSHAN, E. C. G. Completely positive dynamical semigroups of n-level systems. **Journal of Mathematical Physics**, v. 17, p. 821–825, 1976.

HEISENBERG, W. Über den anschaulichen Inhalt der quantentheoretischen Kinematik und Mechanik. **Zeitschrift fur Physik**, v. 43, p. 172–198, 1927.

JAMIOŁKOWSKI, A. Linear transformations which preserve trace and positive semidefiniteness of operators. **Reports on Mathematical Physics**, v. 3, p. 275–278, 1972.

JEKNIC-DUGIC, J.; ARSENIJEVIC, M.; DUGIC, M. Invertibility as a witness of markovianity of the quantum dynamical maps. 2021.

JOZSA, R. Fidelity for mixed quantum states. **Journal of Modern Optics**, Taylor Francis, v. 41, p. 2315–2323, 1994.

KLIESCH, M.; KUENG, R.; EISERT, J.; GROSS, D. Improving compressed sensing with the diamond norm. **IEEE Transactions on Information Theory**, Institute of Electrical and Electronics Engineers (IEEE), v. 62, p. 7445–7463, 2016.

LANDAUER, R. Information is physical. **Physics Today**, v. 44, p. 23–29, 1991.

LANDI, G. T.; PATERNOSTRO, M. **Irreversible entropy production, from quantum to classical**. 2020.

LI, C.-F.; GUO, G.-C.; PIILO, J. Non-markovian quantum dynamics: What does it mean? **EPL (Europhysics Letters)**, IOP Publishing, v. 127, p. 50001, 2019.

LI, C.-F.; GUO, G.-C.; PIILO, J. Non-markovian quantum dynamics: What is it good for? **EPL (Europhysics Letters)**, IOP Publishing, v. 128, p. 30001, 2020.

LI K., W. A. squashed entanglement, k-extendibility, quantum markov chains, and recovery maps. **Found Phys 48**, p. 910–924, 2018.

LIEB, E. H.; RUSKAI, M. B. Proof of the strong subadditivity of quantum-mechanical entropy. **Journal of Mathematical Physics**, v. 14, p. 1938–1941, 1973.

LINDBLAD, G. On the generators of quantum dynamical semigroups. **Communications in Mathematical Physics**, Springer, p. 119–130, 1976.

NEUMANN, J. v. Thermodynamik quantenmechanischer gesamtheiten. **Nachrichten von der Gesellschaft der Wissenschaften zu Göttingen, Mathematisch-Physikalische Klasse**, p. 273–291, 1927.

NEUMANN, J. v. **Mathematische Grundlagen der Quantenmechanik**. [S.l.: s.n.], 1933.

NIELSEN, M. A.; CHUANG, I. L. **Quantum Computation and Quantum Information**. [S.l.]: Cambridge University Press, 2000.

PETZ, D. Sufficient subalgebras and the relative entropy of states of a von neumann algebra. **Comm. Math.Phys.**, v. 105, p. 123–131, 1986.

PETZ, D. Sufficiency of channels over von neumann algebras. **Quart. J. Math.Oxford Ser. (2)**, v. 39, p. 97–108, 1988.

PETZ, D. Monotonicity of quantum relative entropy revisited. **Reviews in Mathematical Physics**, 2003.

PRITCHARD, D. E. Cooling neutral atoms in a magnetic trap for precision spectroscopy. **Phys. Rev. Lett.**, American Physical Society, v. 51, p. 1336–1339, 1983.

RIVAS, A.; HUELGA, S. F. Open quantum systems. **Springer Briefs in Physics**, Springer Berlin Heidelberg, 2012.

RIVAS, A.; HUELGA, S. F.; PLENIO, M. B. Entanglement and non-markovianity of quantum evolutions. **Phys. Rev. Lett.**, American Physical Society, v. 105, p. 050403, 2010.

RIVAS, ; HUELGA, S. F.; PLENIO, M. B. Quantum non-markovianity: characterization, quantification and detection. **Reports on Progress in Physics**, v. 77, p. 094001, 2014.

RUSKAI, M. B. Beyond strong subadditivity? improved bounds on the contraction of generalized relative entropy. **Reviews in Mathematical Physics**, v. 06, p. 1147–1161, 1994.

SCHUMACHER, B.; WESTMORELAND, M. **Quantum Processes Systems, and Information**. [S.l.]: Cambridge University Press, 2010.

SHANNON, C. E. A mathematical theory of communication. **Bell System Technical Journal**, 1948.

STEVENSON, R. (Director). **Mary Poppins**. [S.l.]: United States, Walt Disney Productions, 1964.

SUDARSHAN, P. M. M. E. C. G.; RAU., J. Stochastic dynamics of quantum–mechanical systems. **Phys. Rev.**, v. 121, 1961.

VEGA, I. de; ALONSO, D. Dynamics of non-markovian open quantum systems. **Rev. Mod. Phys.**, American Physical Society, v. 89, p. 015001, 2017.

WATROUS, J. Simpler semidefinite programs for completely bounded norms. **arXiv e-prints**, p. arXiv:1207.5726, 2012.

WOLF, M. M.; CIRAC, J. I. Dividing quantum channels. **Communications in Mathematical Physics**, Springer Science and Business Media LLC, v. 279, p. 147–168, 2008.

ŻYCZKOWSKI, K. ; SOMMERS, H.-J. Average fidelity between random quantum states. **Phys. Rev. A**, American Physical Society, v. 71, p. 032313, 2005.

APPENDIX A - RANDOM MIXED STATE GENERATION

The generation of a random mixed state was made computationally using Mathematica program. We build a function that generates a random mixed state using an uniform distribution $\mathcal{U}\{a, b\}$, whose values are represented by numbers in an interval $[a, b]$, so that a and b become the main parameters of the distribution. This distribution is a symmetric probability distribution, whose values are equally likely to be observed.

This is quite useful since we want to achieve all states of the Bloch sphere, and consequently we are not privileging one region more than the other. This gives us a faithful range of mixed states of the sphere.

APPENDIX B - CONVERGENCE TEST

In statistical analysis, the convergence of random variables to some limit random variable is an important concept and with lots of applications in probability theory, and in the study of probability distribution describing an unknown phenomena. The idea can be formalized that a sequence of essentially random or unpredictable events can sometimes be expected to converge into some behavior that is essentially unchanging or settle down to a limiting constant value. Mathematically we expect that the variance $Var(X)$

$$Var(X) = \sum_{i}^{n} \frac{(X_i - \bar{X})^2}{n-1}$$

decreases to a negligible value or even zero. Where the $X_{i i=0}^{n}$ are the outcomes of some random variable X and $\bar{X}$ is the mean value. It measures how far a set of numbers is spread out from their mean value.

In Fig. 25, we noticed that the difference between the values of the fidelity on average $\bar{F}$ becomes negligible when we take a sample of bigger or equal than 10^4 initial states corresponding to the state space of the Bloch sphere. We opted to choose this value because it is sufficient and necessitates a smaller simulation time compared to a bigger sample of states.

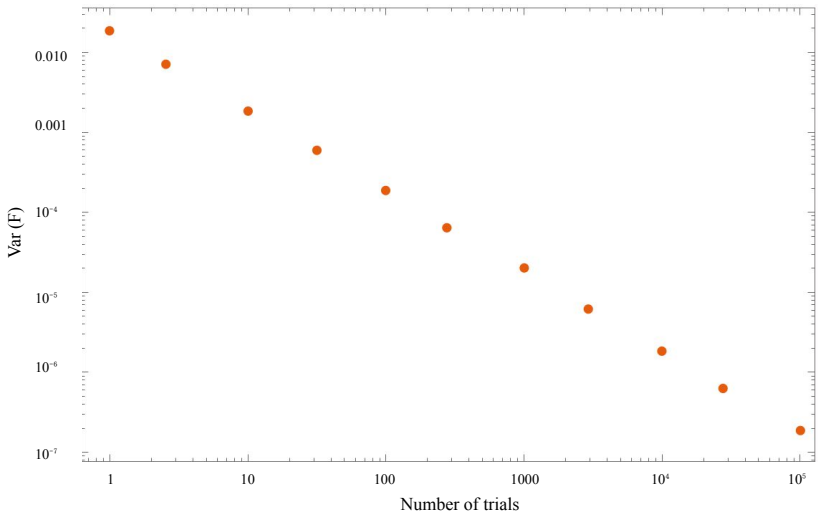

Figure 25 – Decay of the variance with the increase of the number of initial states as sample space.

APPENDIX C - IDENTITY CHANNEL

This section demonstrates the calculation of the fidelity on average without applying the Petz recovery map. Instead, we use the well known Identity channel $\mathcal{I}$. Given a quantum state ρ, the action of this channel is given by

$$\mathcal{I}(\rho) = \rho. \tag{83}$$

Based on the scheme of Fig. 9, we need to calculate the fidelity between the initial state and the evolved state ρ_t, since according to Eq. 83, the state remains itself $\mathcal{I}(\rho_t) = \rho_t$. In order to obtain the mean value of a function $f(u, v, w)$ we compute the integral of f over a region $\mathcal{D}$, and divided the result by the volume of $\mathcal{D}$ as can be seen here

$$\text{Mean value} = \frac{1}{V} \iiint_D f(u, v, w)\, du\, dv\, dw \tag{84}$$

With this idea in mind, we calculate the function $F(\rho_0, \rho_t)$ that is the fidelity over all the states of the Bloch sphere. Each state can be written in spherical coordinates $\rho = \rho(r, \theta, \phi)$. In this case the region is a sphere of radius 1. The fidelity on average is then given by

$$\bar{F} = \frac{1}{\frac{4\pi}{3}} \int_0^1 \int_0^\pi \int_0^{2\pi} F(\rho_0, \rho_t) r^2 \sin\theta\, dr\, d\theta\, d\phi, \tag{85}$$

where $V = 4\pi/3$ the volume of a unitary sphere, $r^2 \sin\theta$ is the Jacobian in spherical coordinates. This calculation is made for each one of the quantum channels.